METALLIC COATING THICKNESS ASSESSMENT OVER NONMAGNETIC METALS USING EDDY CURRENT TECHNOLOGY

by

Zain Ali Ansari

A Thesis Presented to the Faculty of the
American University of Sharjah
College of Engineering
in Partial Fulfillment
of the Requirements
for the Degree of

Master of Science in
Mechanical Engineering

Sharjah, United Arab Emirates

April 2019

Approval Signatures

We, the undersigned, approve the Master's Thesis of Zain Ali Ansari

Thesis Title: Metallic coating thickness assessment over nonmagnetic metals using eddy current technology

Signature	**Date of Signature** (dd/mm/yyyy)
_____	_____
Dr. Bassam Abu-Nabah Assistant Professor, Department of Mechanical Engineering Thesis Advisor	
_____	_____
Dr. Maen Alkhader Associate Professor, Department of Mechanical Engineering Thesis Co-Advisor	
_____	_____
Dr. Mohammad Jaradat Associate Professor, Department of Mechanical Engineering Thesis Committee Member	
_____	_____
Dr. Amer Zakaria Assistant Professor, Department of Electrical Engineering Thesis Committee Member	
_____	_____
Dr. Mamoun Abdel-Hafez Head, Department of Mechanical Engineering	
_____	_____
Dr. Lotfi Romdhane Associate Dean for Graduate Affairs and Research College of Engineering	
_____	_____
Dr. Naif Darwish Acting Dean, College of Engineering	
_____	_____
Dr. Mohamed El-Tarhuni Vice Provost for Graduate Studies	

Acknowledgement

I would like to begin by thanking Allah, for without his will none of this work would have been possible. Secondly, I would like to express my utmost gratitude to my advisors Dr. Bassam Abu-Nabah and Dr. Maen Alkhader. Their continuous perseverance throughout this research enabled me to push my boundaries and discover abilities I never thought I had. Thirdly, I would like to thank my parents and my sister for the continuous support and prayers which helped me continue this effort with the dedication I had throughout my work. I would also like thank all my professors who have taught me, both at the undergraduate and graduate level with exemplary teaching methods and skills.

These last couple of years have been really challenging for me. The support of my friends was extremely helpful throughout my academic journey. I would like to thank each and every one of my friends who have been by my side throughout my time spent in this prestigious university. Their support is greatly appreciated and I consider myself extremely blessed to be surrounded by such company. This research effort could not have been possible without the support of these extremely special people. Finally, I would like to thank the American University of Sharjah for granting me the Graduate Teaching Assistantship which helped me a great deal financially while also giving me the opportunity to work with various faculty members and students in my department.

Dedication

To my family for always bringing out the best in me…

Abstract

Recent improvements in apparent eddy current conductivity (AECC) spectroscopy lends itself as a practical approach to assess metallic coating thicknesses over nonmagnetic metals. It can potentially offer one-order of magnitude improvement in coating thickness estimation when compared to existing phase-sensitive single-frequency and impedance-based multiple-frequency measurement systems. Existing methods require the lift-off distance between the sample and calibration blocks to be consistent to ensure that the obtained measurement is accurate. Building on AECC measurement capabilities, which offer a significantly reduced sensitivity to those deviations, a robust forward and inverse approach is developed in this thesis using single-frequency AECC measurements. The proposed inversion algorithm is developed using the Bisection method, a numerical interpolation technique used for approximating solutions where determining the exact answer is not possible. The logarithmic nature of the problem as well as the requirement of two initial guesses to start the iteration process while covering the entire coating thickness range of interest further justifies the use of the selected method. This not only reduces AECC spectroscopy measurements from a broad frequency range to single-frequency measurements, but also reduces the coil diameter by one-order of magnitude while complying with the plane-wave approximation in the lift-off range of interest. The accuracy in estimating coating thicknesses using both single- and multiple-frequency AECC measurement techniques are compared numerically and experimentally in agreement with the plane-wave approximation for different coating thicknesses relevant to the industry. It is demonstrated that AECC measurement technology delivers 3% uncertainty in metallic coating thickness estimation over nonmagnetic metals in a ±25.4 μm liftoff range. This makes it a practical approach to replace commercially available measurement systems while offering one-order of magnitude improvement in coating thickness estimation.

Keywords: ***Nonmagnetic; coating thickness; eddy current; nondestructive testing; inversion.***

Table of Contents

List of Figures

List of Tables

Chapter 1. Introduction

In this chapter, a short introduction is provided about the rising demand of titanium and nickel alloys and the reasons why they are becoming so popular in the area of weld overlay and metal spraying technologies. Following this, the problem at hand is addressed as well as the research contribution. Finally, a general organization of the thesis proposal is presented.

1.1. Overview

With the use of nickel and titanium alloys, weld overlay and metal spraying technologies deliver attractive solutions to the industry as they exhibit excellent corrosion resistance behaviour and high strength characteristics while operating at high temperatures [1–3]. The implementation of these dissimilar metal-joining processes has gained rapid popularity at design and manufacturing levels in Aviation and Oil and Gas industries as they deliver cost-effective solutions with the rising cost of these alloys. The application of these technologies has also been extended to the service sector of these industries in support of repairing their damaged components. This mandates the use of reliable and practical non-destructive evaluation techniques to assess metallic coating thicknesses over nonmagnetic metals.

Recent advancements in these technologies have not only been able to deliver cost-effective solutions, but they have also been able to provide the protective layer and surface characteristics which are required for the functionality of the product. Moreover, the requirement of these metals to aid in the repair of damaged components, especially for large structures has further increased their applications in the service sector for these industries. This has increased the demand for a practical nondestructive evaluation technique which could assess the coating thickness of metallic coating over nonmagnetic metals.

1.2. Thesis Objectives

The motivation that drives this research is the lack of available non-destructive techniques currently present to assess metallic coating over nonmagnetic metals. The main objective of this thesis is to establish a reliable and accurate non-destructive coating thickness measurement technique for this purpose. This will be achieved using the so called Apparent Eddy Current Conductivity (AECC). This work will then be validated theoretically, numerically and experimentally with the AECC measurements

taken at a single frequency instead of covering a broad range of frequencies, which has been the case so far.

1.3. Research Contribution

The contributions of this research can be summarized as follows:

- Propose a new method of measuring metallic coating thickness over nonmagnetic metals using AECC measurements at a single frequency.
- Optimize the frequency at which AECC measurements will be taken for a given coating/substrate combination.
- Reduce the coil diameter required to take AECC measurements.
- Improve the calibration process of AECC measurement by reducing the number of calibration blocks required.
- Propose a new AECC-based inversion algorithm to assess coating thicknesses and validate the results both numerically and experimentally with those obtained using plane-wave approximation.

1.4. Thesis Organization

The rest of the thesis is organized as follows: Chapter 2 provides background information of existing standards used in evaluating coating thickness as well as existing methods that are available and why they are insufficient. Building on the previous spectroscopy AECC-based inversion model, a new model is presented in Chapter 3 and is validated experimentally in Chapter 4. Finally, Chapter 5 highlights the conclusion and provides future prospects for the technology.

Chapter 2. Background and Literature Review

This chapter addresses the current status of eddy currents including the standards that are used at present and assess coating thicknesses of various coating/substrate combinations. It also provides an insight into the eddy current forward problem and the manner through which it can be estimated both analytically and numerically. Finally, it discusses the current status of eddy current technologies and the lack of existing inverse eddy current models to assess rectangular coating thickness profiles.

2.1. Background

In compliance with the International Organization for Standardization (ISO), the assessment of a metallic or nonmetallic coating thickness over a metallic or magnetic substrate is controlled with different standards made available to the industry using magnetic induction and eddy current technologies. Phase-sensitive eddy current technique is typically implemented to assess metallic coating thicknesses over nonmagnetic metals per ISO 21968 [4]. It calls for calibrating the eddy current measurement system over nonmagnetic metal coating/substrate calibration blocks of different coating thicknesses to establish a probe characteristic curve. However, coating and substrate conductivities delivered in manufacturing processes slightly vary from those used in the calibration blocks. This can adversely affect the accuracy of estimating coating thicknesses as eddy current measurements over coated structures deviate from the probe characteristic curve. Additionally, accuracy in coating thickness estimation requires placing the probe over a coated structure at a lift-off distance consistent with the one used in establishing the probe characteristic curve. This can be accounted for with the implementation of a lift-off compensation procedure, which calls for a new probe characteristic curve measured at a controlled lift-off distance consistent with that used over the coated structure. This is typically arranged by placing a plastic shim of a known thickness, which is equivalent to the lift-off distance of interest, between the probe and the coated calibration blocks. In all cases, lift-off over the calibration blocks and coated structure shall be consistent to deliver the accuracy needed in estimating coating thicknesses.

Assuming a nonmagnetic-layered structure, Dodd and Deeds' exact solutions to the forward eddy current problem [5, 6] can be used for coating thickness estimation

[7] assuming pure inductive coupling. In the forward model, the analytical solution of the frequency-dependent coil impedance can be determined with the input of numerous electromagnetic constraints such as conductivities of the coated/substrate structure, coil parameters, lift-off distance, lead wire lengths, etc. [5–8]. Alternatively, commercially available tools such as COMSOL, Vic-3D, etc. can be used to estimate the complex impedance coil spectrum numerically [8, 9]. These analytical and numerical forward models lend themselves for impedance-based inversion algorithm solutions to assess metallic coating thicknesses from the frequency-dependent coil impedance $Z(f)$ measured over coated structures [7]. It further requires measuring the complex coil impedance spectrum over the nonmagnetic substrate $Z_0(f)$ to estimate the impedance change $\Delta Z(f) = Z(f) - Z_0(f)$ needed to assess nonmagnetic coating thicknesses [7]. Other than the need to measure the impedance change in a relatively broad frequency range, these measurements are sensitive to conductivity deviations of substrates in coated structures relative to the conductivity of the uncoated substrate used as a reference block. Furthermore, the dependency of the impedance-based model on lift-off makes the technique less practical as it requires matching the lift-off over the coated structure with that used over the reference block to deliver 10% uncertainty in coating thickness estimation. Based on numerical simulations of impedance-based forward and inverse models, a ±25.4 μm lift-off deviation from the reference block delivers 30% uncertainty in coating thicknesses estimation [10]. Alternatively, hyperbolic regression considering the lift-off effect, can be adopted for a more flexible calibration method to evaluate the relationship between the coil impedance and coating thicknesses with higher accuracy [11]. To overcome time limitations set with the use of eddy current coil impedance spectroscopy, time-domain analysis using pulsed eddy current (PEC) technology presents a promising solution in assessing coating thicknesses with speed in such nonmagnetic structures. Unfortunately, PEC delivers 13% uncertainty in estimating metallic coating thicknesses over nonmagnetic substrates mainly due to the dependency of the forward model on lift-off [12]. Emerging technologies such as PEC and electromagnetic optical imaging techniques need further investigation in the fields of coating thickness assessments [13].

Recent developments in eddy current capabilities allow capturing apparent eddy current conductivity (AECC) spectrums with relatively high accuracy and precision [14]. Implementing an optimized coil design, together with a high-order calibration

algorithm, minimizes AECC sensitivity to sample conductivity and lift-off deviations from those used over the calibration blocks. It allows the measurement system to operate up to 80-100 MHZ with less than 0.1% uncertainty in AECC measurements within ± 5% conductivity and ± 25 μm lift-off ranges [15–26]. The later represents a practical lift-off variation just from placing the probe alone over the coated sample. More importantly, the accuracy in estimating the AECC spectrum does not depend on the conductivity of the substrate used as a reference block following the impedance-based forward model. Instead, different uncoated conductivity calibration blocks are used to bracket the apparent conductivity of interest. As a forward model, this makes AECC-based spectroscopy a suitable replacement to overcome the impedance-based measurement limitations. Until recently, AECC-based inversion models require continuous and smooth depth-dependent conductivity profiles [9, 18], which do not apply to coated structures of rectangular conductivity profiles. Recent developments in AECC-based inversion models demonstrated the potential capabilities of using the forward AECC spectroscopy to assess metallic coating thicknesses over nonmagnetic metals [10]. It can deliver one order of magnitude improvement in coating thickness assessment over existing impedance-based inversion models in a lift-off range of ±25.4 μm. Unfortunately, the technique requires capturing the AECC spectrum over a broad frequency range using a relatively large coil design (D = 50 mm) to meet the plane-wave approximation [10]. This makes the technique relatively unpractical and difficult to compete with potential solutions offered using PEC technology [12] or frequency scanning using eddy current grid technique [27, 28], which uses a significantly smaller coil diameter. However, AECC-based models not only present a new way of estimating coating thicknesses of rectangular conductivity profiles but they also decrease the measurement sensitivity to conductivity and lift-off deviations from those used over the calibration blocks.

2.3. Forward Eddy Current Problem

Metallic coatings over nonmagnetic metals represent nonmagnetic-layered structures with depth-dependent inhomogeneous conductivity profiles. At a given inspection frequency, the previously mentioned AECC is defined as the conductivity of an equivalent homogeneous medium producing similar complex coil impedance over a depth-dependent inhomogeneous conductivity profile [21]. Estimating the AECC for a

given coating/substrate combination can be achieved directly using the plane wave approximation or indirectly through numerical and experimental means.

2.3.1. Direct approach. The use of the plane-wave approximation to estimate the AECC spectrum of a known depth dependent conductivity profile is done by equating the reflection coefficient $R(f)$ of the inhomogeneous conductivity profile to that of an equivalent homogeneous conductivity sample at the same frequency [9]. Here the AECC of the inhomogeneous conductivity profile is represented by the equivalent homogenous one at the given frequency. For a known conductivity profile that only changes with depth, the inhomogeneous half-space electromagnetic surface impedance $Z(0)$ can be estimated with the application of the plane-wave approximation by continuous repetition of the wave-guide equation starting deep enough below the surface where electric conductivity variation is negligible [9]. Following this the plane-wave reflection coefficient $R(f)$ at the surface of the conductor is calculated by the formula mentioned below:

$$R(f) = \frac{\eta_0 - \xi(0)}{\eta_0 + \xi(0)}, \tag{1}$$

where the intrinsic impedance of free space and the electric surface impedance of the conducting half space are denoted by η_0 ($\approx 377\ \Omega$) and $\xi(0)$ respectively. To evaluate AECC at any given frequency, the following equation is used [9]:

$$\Gamma(f) \approx \frac{4\pi f \mu_i \varepsilon_0}{\mu_0 [1 - \mathrm{Re}\{R(f)\}]^2}, \tag{2}$$

where ε_0 and μ_0 are the electric permittivity and magnetic permeability of a vacuum, respectively, and μ_i is the magnetic permeability of the intact conductor. The magnetic permeability of the intact conductor equals that of a vacuum, i.e., $\mu_i \approx \mu_0$ as this research only targets metals that are nonmagnetic.

Figure 1 shows the advantage of applying the plane-wave approximation over (a) a smooth and continuous conductivity profile to estimate (b) its AECC spectrum, and (c) a rectangular conductivity profile to estimate (d) its AECC spectrum. The plane-wave approximation was validated previously covering this range of conductivity variation (≈ 1%) using Vic-3D [9]. Before utilizing it in the new AECC-based inversion model, the plane-wave approximation must be validated for the coating/substrate

conductivity variations (≈ 56%) of interest due to the advantages offered through it as a direct forward approach. More importantly, adjustments need to be made to the indirect forward simulation model so that it can cover this level of conductivity variations. These indirect simulations will be used as “measured” AECC spectrums to validate the new AECC-based inversion model, which is discussed in the following sub-section.

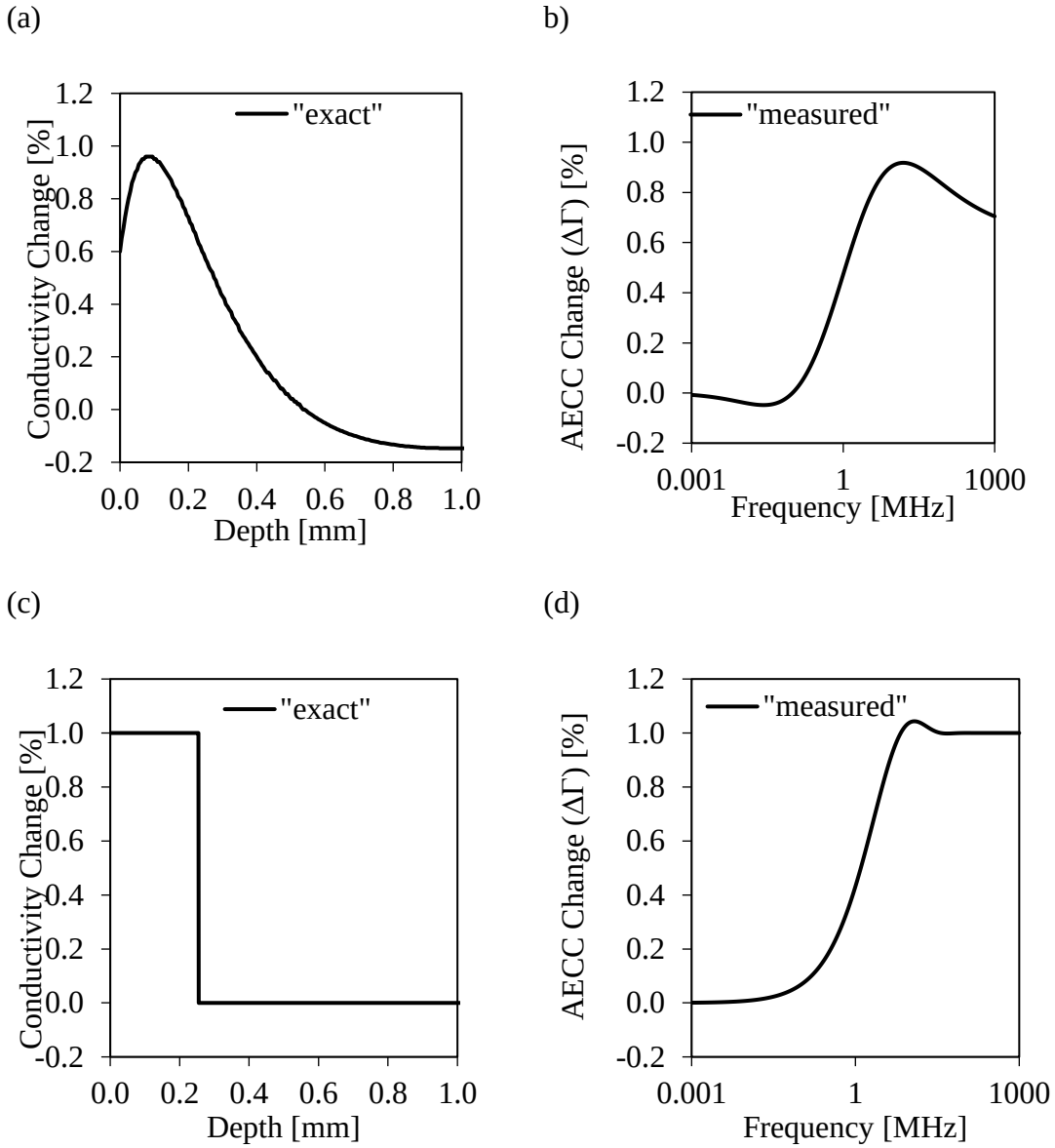

Figure 1. The plane-wave approximation over a continuous conductivity profile to estimate its AECC change, and a rectangular conductivity profile to estimate its AECC change [10].

2.3.2 Indirect approach. From a practical perspective, AECC spectroscopy can be indirectly estimated using two separate steps. The first step requires establishing a methodology to estimate the complex coil impedance spectrum Z(f) at a given lift-off distance. For a given coil design, this step can be accomplished theoretically [5–7], numerically [30–37] and experimentally [7, 17, 39]. In this study, the previously demonstrated capabilities of COMSOL simulations is used to execute this step numerically [10]. The second step requires a system calibration to evaluate AECC from a coil complex impedance measured or simulated over an inhomogeneous sample at a given frequency. In this step, coil complex impedances measured or simulated over two homogeneous calibration blocks with (l = s) and without (l = 0) lift-offs are needed to bracket the coil complex impedance measured or simulated over the inhomogeneous sample at an unknown lift-off distance within the calibration range. Implementing a simple four-point linear interpolation algorithm can be used to estimate the AECC at a given frequency.

This is a significant deviation from phase-sensitive or impedance-based calibration techniques, which call for coating/substrate calibration blocks with different coating thicknesses or an uncoated reference substrate, respectively. In the latter two cases, any deviation in the conductivity of the nonmagnetic-layered structure from the conductivity of the calibration block(s) can adversely affect the accuracy of coating thickness estimation. This is not the case in assessing the AECC of a nonmagnetic-layered structure as the measurement itself captures a physical property of the sample rather than the coil complex impedance alone [30]. A recent development in coil designs and calibration algorithms used in high-frequency AECC spectroscopy reduced the measurement sensitivity to as low as 0.1% in a lift-off range of ±25.4 μm [17]. The capabilities offered through AECC technology makes it a suitable technique to be leveraged for coating thickness estimation.

The robustness of using AECC spectroscopy has been previously established over nonmagnetic metals assessing depth-dependent conductivity variations up to 3% due to surface enhancement methods such as shot peening and low plasticity burnishing [9, 18], and the loss of AECC due to surface roughness introduced from shot peening [39]. The capability of AECC spectroscopy to cover a broader conductivity variation

(≈ 56%) has been recently demonstrated to assess metallic coating thicknesses over nonmagnetic metals [10].

The accuracy in covering this range of AECC variations can be demonstrated for Ti-6Al-4V (σ_c = 1.05 %IACS) 0.5-mm coating thickness over SS304 (σ_s = 2.40 %IACS) semi-infinite substrate shown in Figure 2(a). This was validated directly using the plane-wave approximation (solid line) in close comparison to the indirectly simulated AECC spectrum using COMSOL (markers) as shown in Figure 2(b). In these COMSOL simulations, a relatively large coil diameter (D = 50 mm) was used [10]. In comparison to the plane-wave approximation (solid lines), Figure 3 further demonstrates the potential capabilities of AECC spectroscopy using COMSOL simulations (markers) to cover similar coating/substrate conductivity combination of various coating thicknesses [10].

A schematic representation of AECC COMSOL simulations using 2D axisymmetric model of a coil over metallic nonmagnetic coating/substrate material is shown in Figure 4. This electromagnetic simulation was built using COMSOL's AC/DC module with 1 V excitation to copper coils of different diameters (D). A Ti-6Al-4V coating of σ_c = 1.05 %IACS is simulated over a semi-infinite SS304 substrate of σ_s = 2.40 %IACS. A Ti-6Al-4V coating of σ_c = 1.05 %IACS is simulated over a semi-infinite SS304 substrate of σ_s = 2.40 %IACS. The coating thickness (t_c) ranges between 0.148 and 1.688 mm as previously illustrated in Figure 3 and it is significantly smaller than the substrate thickness (t_s) to meet the plane-wave approximation at low frequencies. Both coating and substrate alloys are nonmagnetic, so their relative magnetic permeability (μ_r) equals to unity. To simulate a realistic eddy current probe, a pull-back distance of 100 µm was set between the lower side of the coil and the lower side of the probe body. The lift-off distance (l), i.e., the separation distance between the lower side of the probe and the coating's top surface, will be simulated in a ± 25.4 µm lift-off range to illustrate the robustness of the proposed technique. Both coated samples and coil designs are surrounded with air.

2.4. AECC-Based Inversion Models

Over the years, two main AECC-based inversions models have been introduced. These are known as the simplistic [9] and iterative models [18]. These models however

were limited to smooth conductivity profiles. For coated structures, the conductivity profiles are rectangular which deems these models redundant.

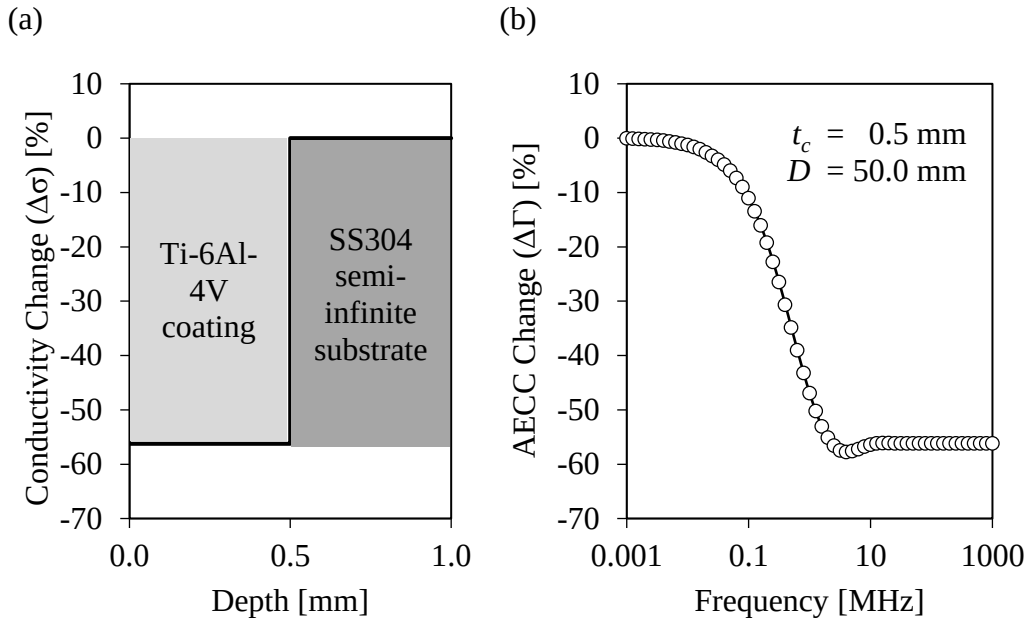

Figure 2. 0.5-mm Ti-6Al-4V coating over SS304 substrate rectangular conductivity change and its corresponding AECC change following the plane-wave approximation (solid line) and COMSOL simulations (empty markers).

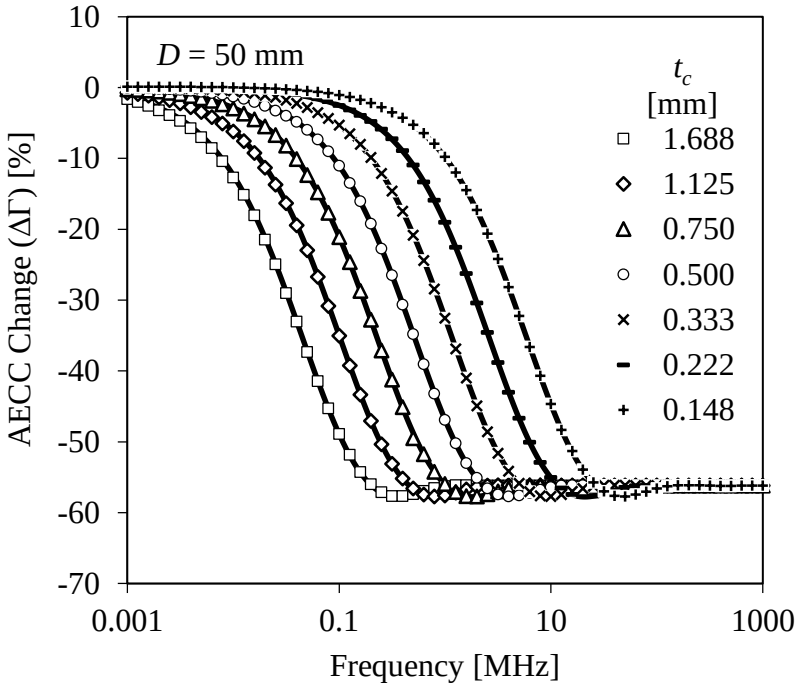

Figure 3 AECC change using the plane-wave approximation (solid lines) and COMSOL simulated 50-mm coil (markers) on different Ti-6Al-4V coating thicknesses over SS304 substrates.

Recently a new AECC based inversion model was created to specifically assess rectangular conductivity profiles using AECC spectroscopy [10].

2.4.1. Simplistic and iterative models. The simplistic model works by roughly assuming that the measured AECC at a given frequency corresponds to the actual conductivity at half the eddy current standard penetration depth as follows:

$$\sigma_0(z = \delta(f)/w) = \Gamma(f), \tag{3}$$

Here the simplistic estimate of electric conductivity at a given depth z is denoted by σ_0 which is roughly estimated using the standard eddy current penetration depth δ. An arbitrary scaling factor w to offer the best overall agreement actual conductivity profile and the inverted one obtained from the simplistic model where w=2. The initial depth-dependent conductivity profile estimated from the simplistic model is denoted by the subscript 0. This will then be used to start the iterative inversion model which is described next.

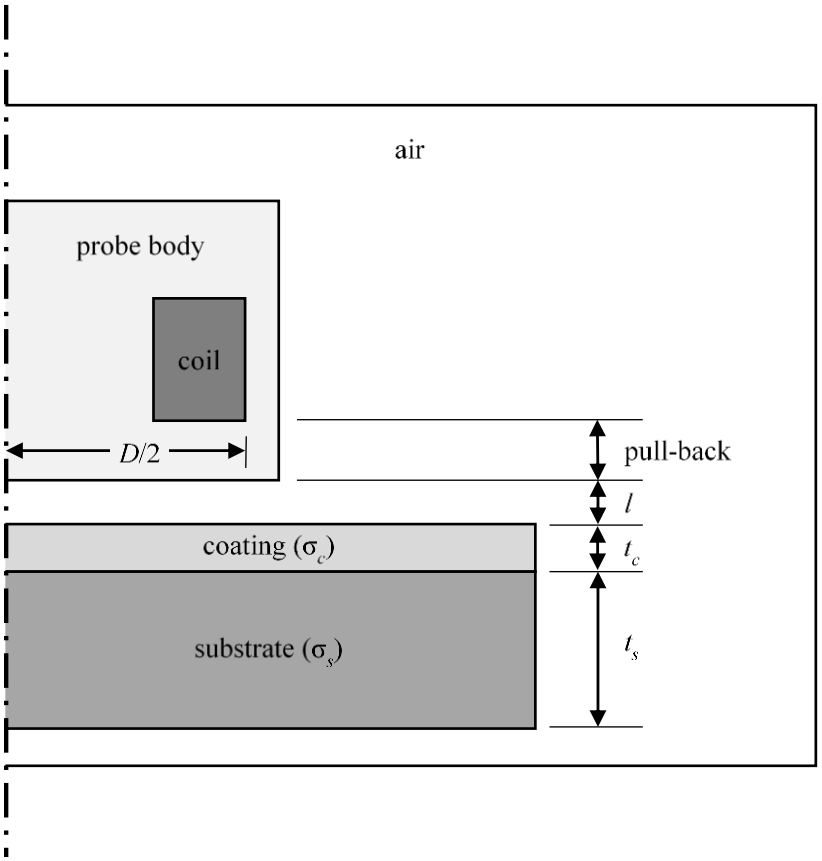

Figure 4. A schematic representation of AECC COMSOL simulations using 2D axisymmetric model of a coil over metallic nonmagnetic coating/substrate material.

Applying the iterative model increases the accuracy that is offered in estimating depth-dependent conductivity profiles. It relies on the simplistic model's potential and the accuracy of the plane-wave approximation in determining the AECC spectrum $\Gamma(f)$ which it uses in a feedback loop as follows.

$$\sigma_{n+1}(z) = \sigma_n(z) + \Gamma(z) - \Gamma_n(z), \tag{4}$$

Where n denotes the iteration number initialized a n=0 to deliver the initial guess of the depth-dependent conductivity profile $\sigma_0(z)$ and its corresponding $\Gamma_0(f)$, which is transformed to get $\Gamma_0(z)$. The measured or simulated AECC spectrum $\Gamma(f)$ belonging to the actual conductivity is transformed to $\Gamma(z)$ and is used as a reference to compensate for the differences encountered in the iterative inversion algorithm for two consecutive conductivity profiles. Following this model, the AECC spectrum for the nth-order $\Gamma_n(f)$ is calculated using the nth-order conductivity profile $\sigma_n(z)$ to get $\sigma_{n+1}(z)$. Taking into consideration, the uncertainty acquired from the AECC measurement, this technique displays quick convergence to the actual continuous conductivity as it only takes two iterations for this to happen.

Figure 5 illustrates the performance of the simplistic and iterative models on the (a) continuous conductivity profile, (b) and its AECC spectrum. The depth dependent conductivity profile $\sigma_0(z)$ is delivered by the 0^{th} iteration following the simplistic inversion model the corresponding AECC spectrum $\Gamma_0(f)$ is simulated following the plane-wave approximation. Implementing the iterative AECC-based model illustrates its ability in capturing the actual "exact" continuous conductivity profiles. The performance of the simplistic and iterative models is also shown for rectangular conductivity profiles in Figure 5, however it can be seen that the deviation of the 0th order conductivity profile $\sigma_0(z)$ from the "exact" rectangular conductivity profile $\sigma(z)$ starts to grow from the very first iteration. The reason for this deviation is mainly due to the nature of AECC spectrums that are continuous regardless of them being measured or simulated. Using them as feedback in Eq. 4 does not allow the model to capture the AECC spectrum of discontinuous depth dependent conductivity profiles. This makes both the AECC-based inversion models unfit for rectangular conductivity profiling.

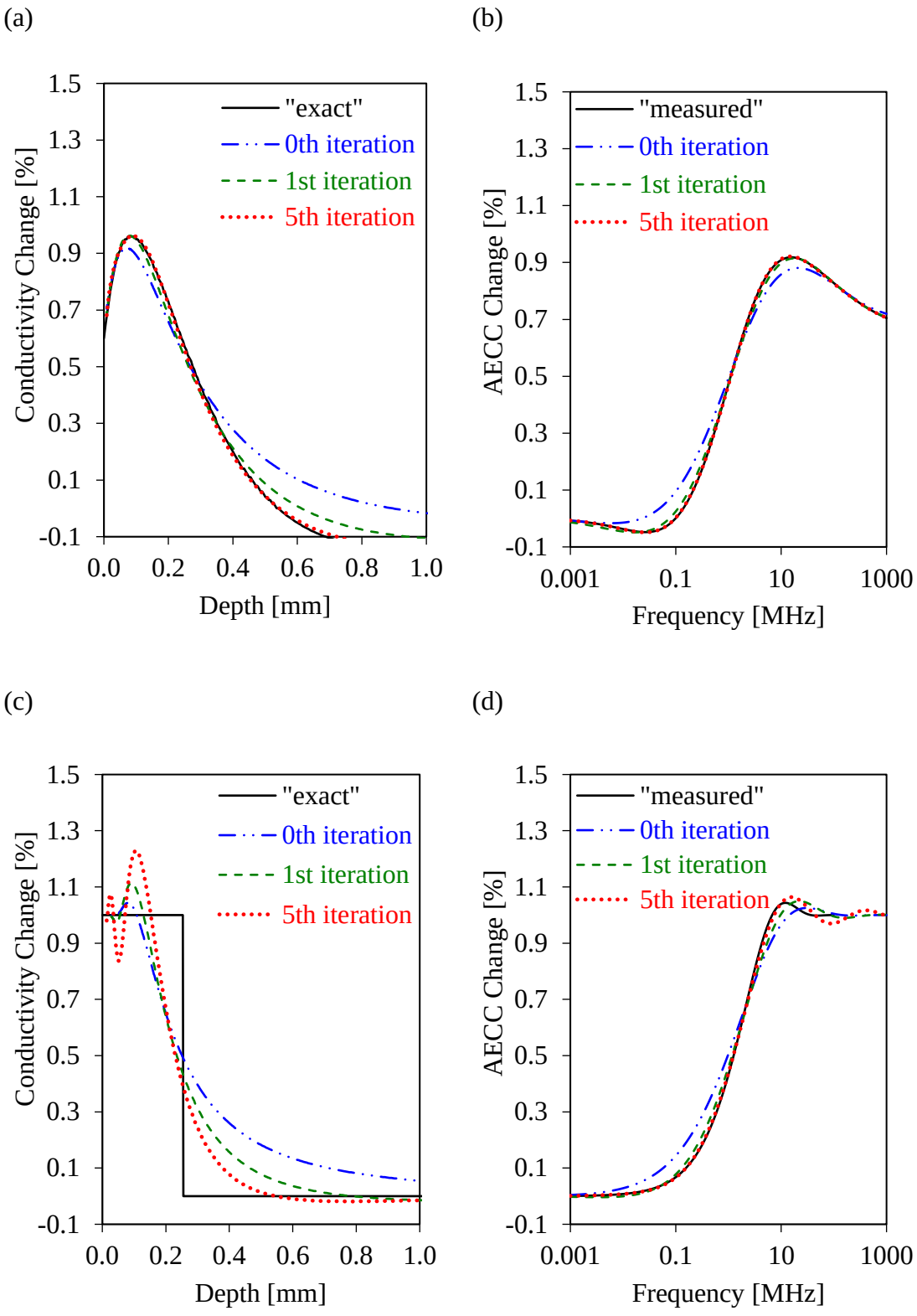

Figure 5. Performance of existing simplistic (0th iteration) and iterative AECC-based inversion models at different iterations on a continuous conductivity profile with its AECC change and a rectangular conductivity profile, and its AECC change [10].

2.4.2 Recently developed spectroscopy AECC-based inversion model. This inversion model uses the rectangular conductivity profile presented in Figure 2(a) is used to simulate the titanium ally Ti-6Al-4V (σ_c = 1.05 %IACS) coating over SS304 (σ_s = 2.40 %IACS) semi-infinite substrate, where the coating thickness is relatively small compared to the overall thickness of the sample. A coating thickness of t_c = 0.5 mm is considered. The capabilities of the model for the same coating/substrate combination with various coating thickness will be illustrated in the upcoming section. The AECC change displayed in Figure 2(b) is simulated using COMSOL and is used as a representation of the "measured" AECC change $\Delta\Gamma_m$ over the coated sample. To proceed with the model, a large enough coil diameter relative to the coating thickness is considered to capture the substrate conductivity at low frequencies. Furthermore, the conductivity variation of the coating material relative to substrate conductivity in the actual "measured" AECC spectrums, is captured accurately by minimizing the coil sensitivity due to lift-off at high frequencies.

The inversion model proposed in this section to assess coating thicknesses of rectangular conductivity profiles counts on the accuracy of the plane-wave approximation in simulating the AECC change, and the convolution of these spectrums at different coating thicknesses to give the best overall agreement with the "measured" one. Figure 6 shows different Ti-6Al-4V coating thicknesses over the SS304 semi-infinite substrate is shown in following the plane-wave approximation to simulate (a) the corresponding AECC change $\Delta\Gamma_t$ for different coating thicknesses, and (b) the deviation of these spectrums from the "measured" one over the 0.5-mm clad thickness, i.e., $\Delta\Gamma_t$ - $\Delta\Gamma_m$.

The proposed inversion algorithm minimizes the deviation's peak $(\Delta\Gamma_t - \Delta\Gamma_m)_{peak}$ to zero by targeting the iteration of different coating thicknesses following the simple secant method as a selected numerical linear interpolation method to determine the coating thickness. The peak deviation of AECC change at different normalized thicknesses relative to AECC change "measured" over the actual coating thickness is displayed in Figure 7. For simplicity this peak deviation $(\Delta\Gamma_t - \Delta\Gamma_m)_{peak}$ as a function of the layer thickness is expressed as $g(t)$. The function $g(t)$ needs to be linearized based on best-fit analysis and to improve the convergence rate of the secant method. This linearization is shown below:

$$g(t) = a\ln(t) + b, \tag{5}$$

Where constants a and b are to be estimated from the best fit analysis, and they need to be updated after every iteration to achieve a higher convergence rate in estimating coating thickness.

Figure 8 shows the proposed flow diagram of the inversion model to assess rectangular conductivity profiles based on the secant method is shown in. This method keeps iterating the thickness based on the secant method's criteria until the best overall agreement is offered between the estimated AECC change $\Delta\Gamma_t$ and the "measured" AECC change $\Delta\Gamma_m$. The initiation of the iteration process, involves the following. First, the coating and substrate conductivities are estimated separately or from the AECC spectrum which is described in the next section. Second, two guesses for the coating thickness are provided which are denoted as t_0 and t_1 respectively, to cover the coating thickness range of interest and start the iteration process. Third, a tolerance level ϵ is specified as a convergence criterion for the estimated thickness. Starting with the first iteration where $n = 1$, AECC change $\Delta\Gamma_{n-1}$ and $\Delta\Gamma_n$ are estimated for coating thicknesses t_{n-1} and t_n, respectively, following the plane-wave approximation. The peak variation between the estimated and measured AECC change for a given thickness i.e., $g(t) = (\Delta\Gamma_t - \Delta\Gamma_m)_{peak}$, is estimated as defined in the linearized equation mentioned above which is updated after each iteration If the $|g(t_{n-1})| > |g(t_n)|$, then t_{n-1} and t_n is swapped for that particular iteration to ensure that the numerical technique reaches convergence. Based on the linear estimate of $g(t)$, t_{n+1} is estimated where $g(t_{n+1}) = 0$. If the absolute peak variation $|g(t_{n+1})|$ is lower than the tolerance level ϵ, then the estimated layer thickness t is t_{n+1}. If that is not the case, then the iterative process is continued until convergence is obtained as defined by the tolerance level ϵ. The following section discusses the assessment of the proposed inversion method over nonmagnetic rectangular conductivity profiles where the accuracy and convergence rate based on "measured" AECC spectrums using the direct and indirect forward approaches are also shown.

2.4.3 Accuracy of the spectroscopy AECC-based inversion model. The first step in starting the iteration process is identifying the conductivities of both the coating σ_c and the substrate σ_s.

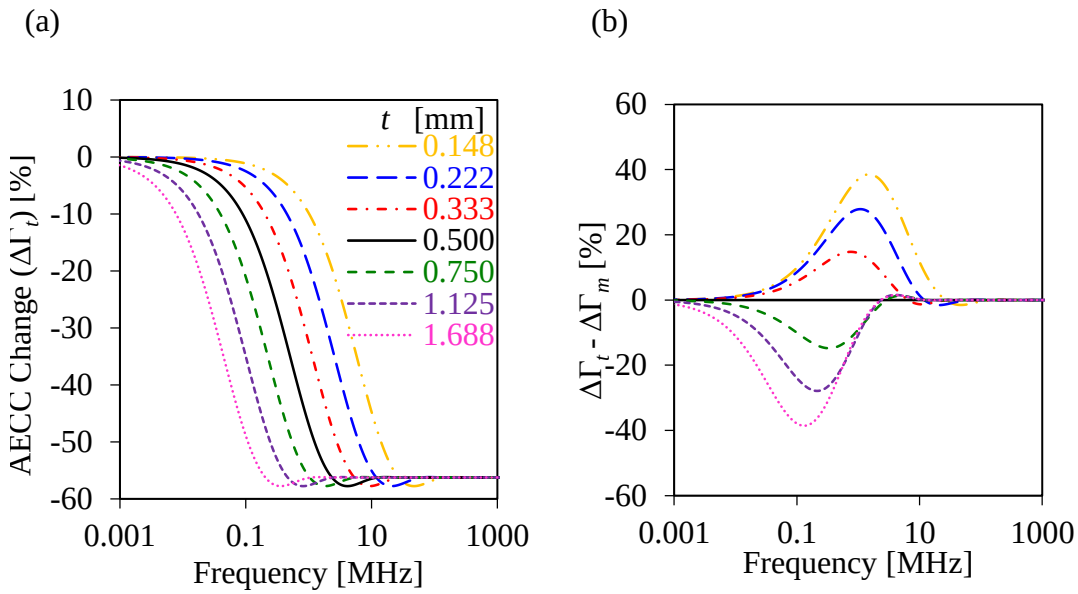

Figure 6. The assessment of different Ti-6Al-4V coating thicknesses over semi-infinite SS304 substrate following the plane-wave approximation to simulate their AECC change ($\Delta\Gamma_t$), and deviations from the "measured" one over the 0.5-mm coating thickness, i.e. $\Delta\Gamma_t - \Delta\Gamma_m$ [10].

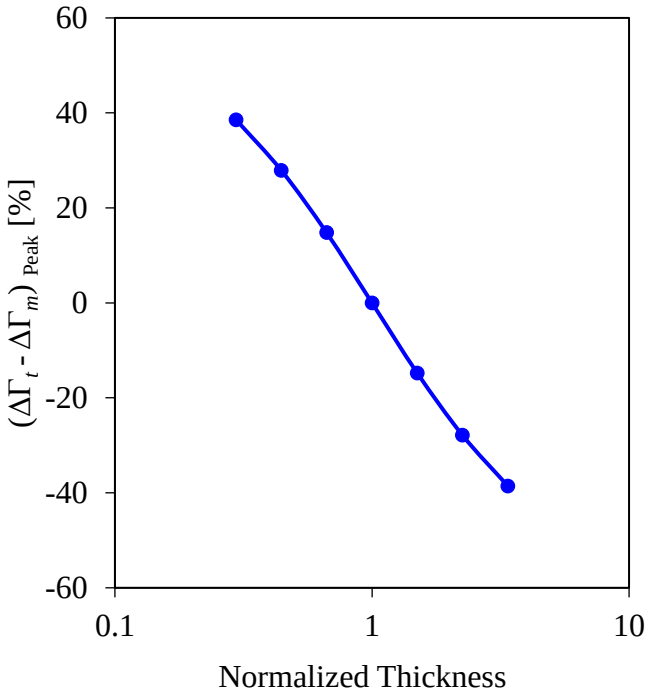

Figure 7. The peak deviations $(\Delta\Gamma_t - \Delta\Gamma_m)$peak at different normalized coating thicknesses [10].

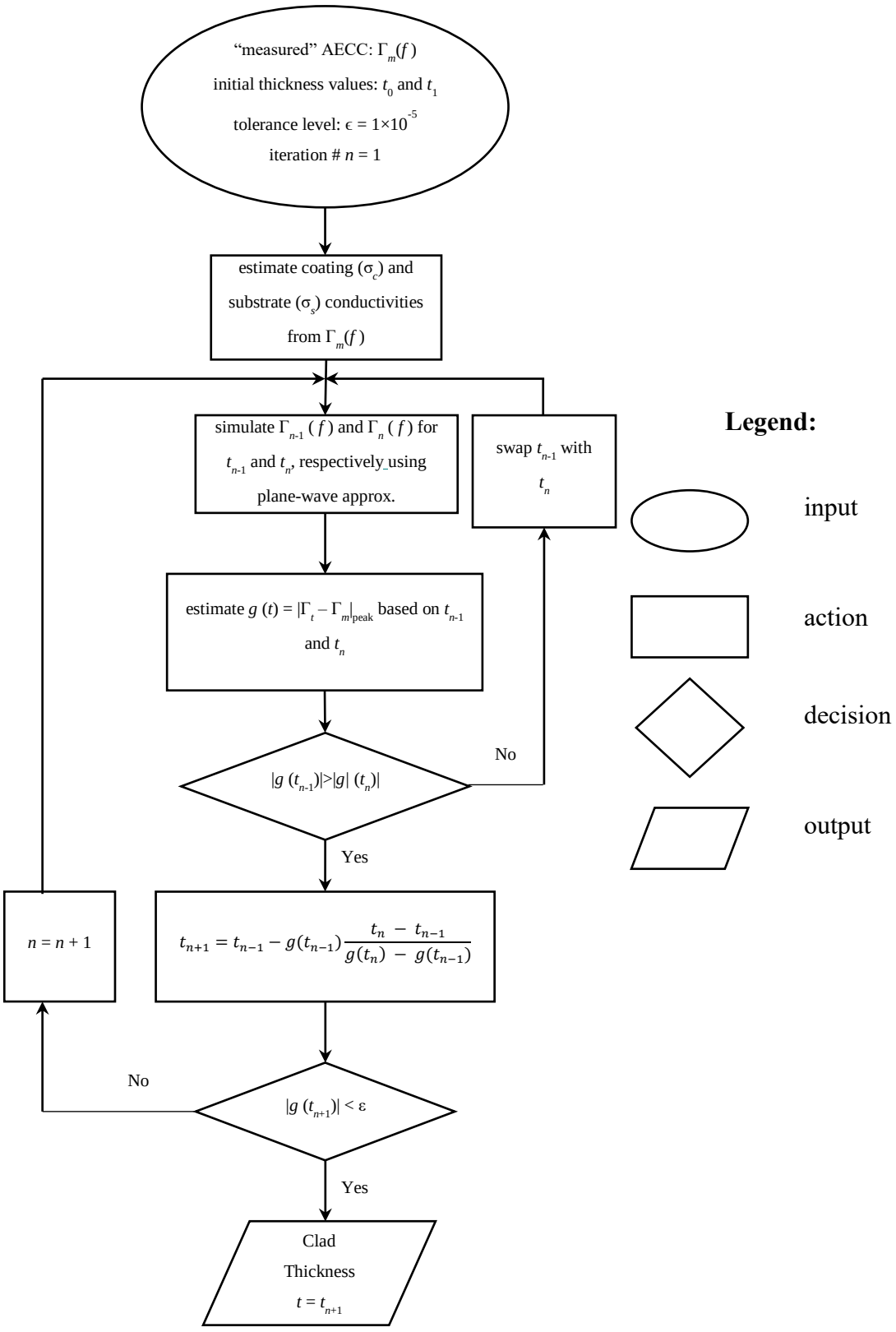

Figure 8. A flow diagram of the existing AECC-based inversion algorithm to assess metallic coating thicknesses over nonmagnetic metals [10].

This can be achieved in two different ways. The conductivities could either be estimated separately or from the "measured" AECC spectrum $\Delta\Gamma_m$. Following the approach of the latter, the conductivity of the coating is captured at relatively high frequencies where the standard penetration depth of eddy current is much smaller than the coating thickness, and the AECC measurements are not sensitive to the conductivity of the substrate. Based on the "measured" AECC change which is shown in Figure 2(b) above 20 MHz the coating conductivity value σ_c is the same as the one shown in the "measured" AECC which is 1.05 %IACS. Conversely, the conductivity of the substrate is captured at relatively low frequencies where the standard penetration depth of eddy currents is relatively higher than the coating thickness. At this frequency range, the AECC measurements are no longer sensitive to the conductivity of the coating. The "measured" AECC change shown in Figure 2(b), the semi-infinite substrate conductivity σ_s equals to the "measured" AECC below 0.001 MHz, i.e., σ_s = 2.40 %IACS. The coating and substrate conductivities can also be measured separately due to the limited capabilities of AECC measurements to cover such a large frequency range with a single coil design. Second, the iteration process of the secant method is started by specifying two initial coating thicknesses. For all practical purposes t_0 = 0.1 mm and t_1 = 4.0 mm which brackets the thickness of interest and starts off the iteration process with a tolerance level of $\epsilon = 1\times10\text{-}5$. Once these parameters are set the program can be implemented. The convergence of rectangular conductivity profiles of 0.5 mm coating thickness as well as the corresponding AECC change, following the plane-wave approximation, are shown in Figure 9(a) and (b) respectively. Figure 9(c) and (d) show the deviation of these spectrums from the "measured" one and the estimated coating thickness at different iterations. Based on this procedure it takes only four iterations for the thickness to converge to the desired value of 0.5 mm at which the corresponding AECC change $\Delta\Gamma_t$ is equivalent to the "measured" AECC change $\Delta\Gamma_m$.

The flexibility of this inversion algorithm is further illustrated by using the same coating/substrate combination at different coating thicknesses. A coating thickness ranging from 0.148 to 1.688 mm is covered with 50% increments. Figure 10 shows the simulated AECC change using the plane wave approximation (solid lines) and COMSOL simulations (empty markers) on rectangular conductivity profiles of Ti-6Al-4V coating over SS304 semi-infinite substrate at different coating thicknesses. In close comparison between the direct and indirect forward models, the results show

the capabilities of the plane-wave approximation as a model to simulate relatively significant AECC changes with high accuracy as it delivers an overall agreement with the results obtained from COMSOL simulations.

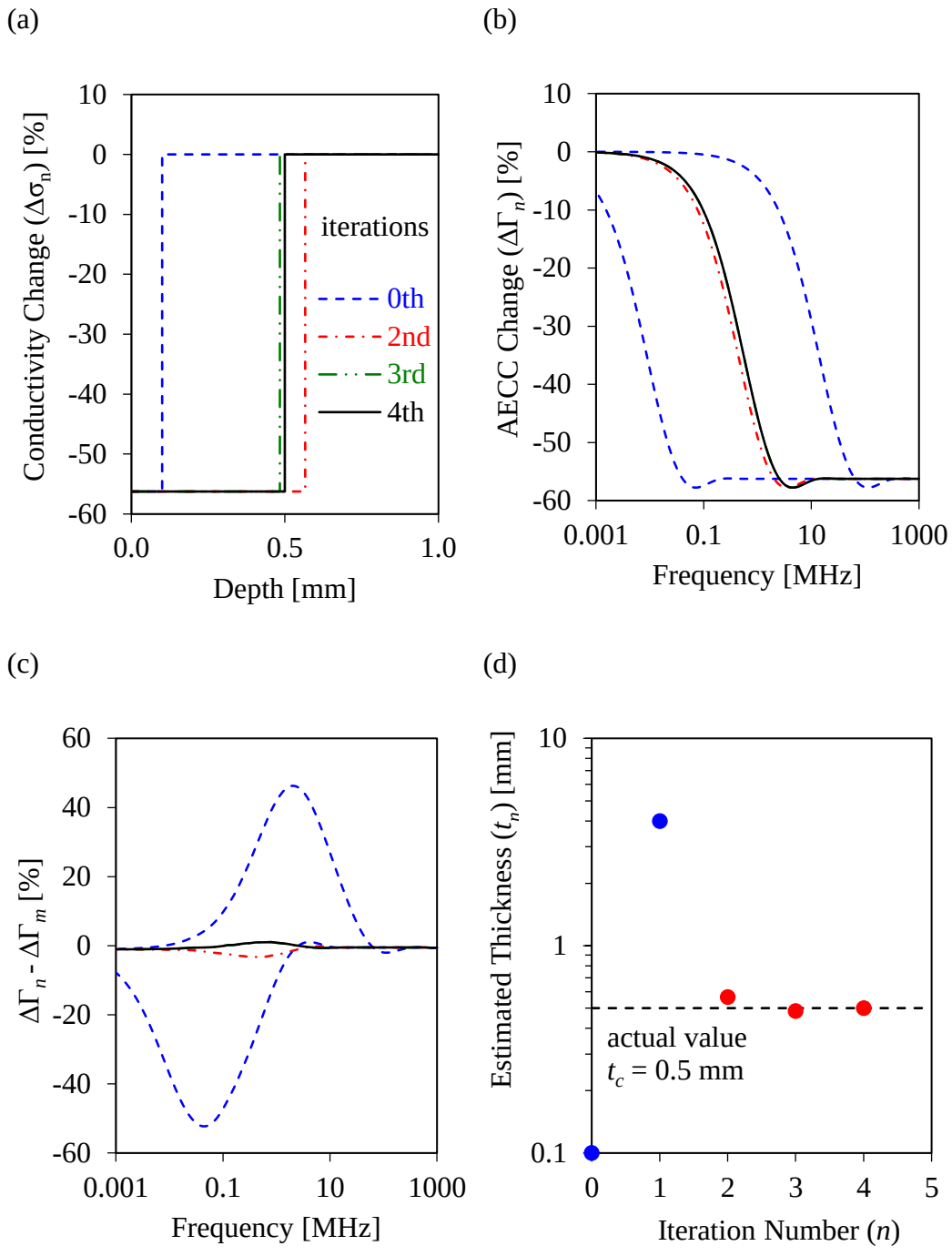

Figure 9. The convergence of rectangular conductivity profiles with their AECC change following the plane-wave approximation and the deviation of these spectrums from COMSOL simulated one converging to the estimated coating thickness [10]

2.5. Comparison Between the AECC and Impedance Based Models

To illustrate the spectroscopy AECC-based inversion algorithm's robustness to lift-off compared to the current impedance based model [7], the coil design *L* used in Ref. [7] was simulated using COMSOL. Using the impedance-based method the simulated resistance change spectrum for different coating thicknesses at 0 μm lift-off is shown in Figure 11(a). Figure 11(b) shows the probe characteristic curves for different coating thicknesses using a crossing frequency of 1Ω. Since this technique is sensitive to lift-off, measurements over coated should be done at the same lift-off at which the probe characteristic curve was established, i.e., 0 μm. Reported experimental results indicate that there is a 10% uncertainty in coating thickness measurements when this approach is used. Consistent lift-off distances between the coated calibration blocks and the coated samples were achieved by spring loading probe while taking measurements [7].

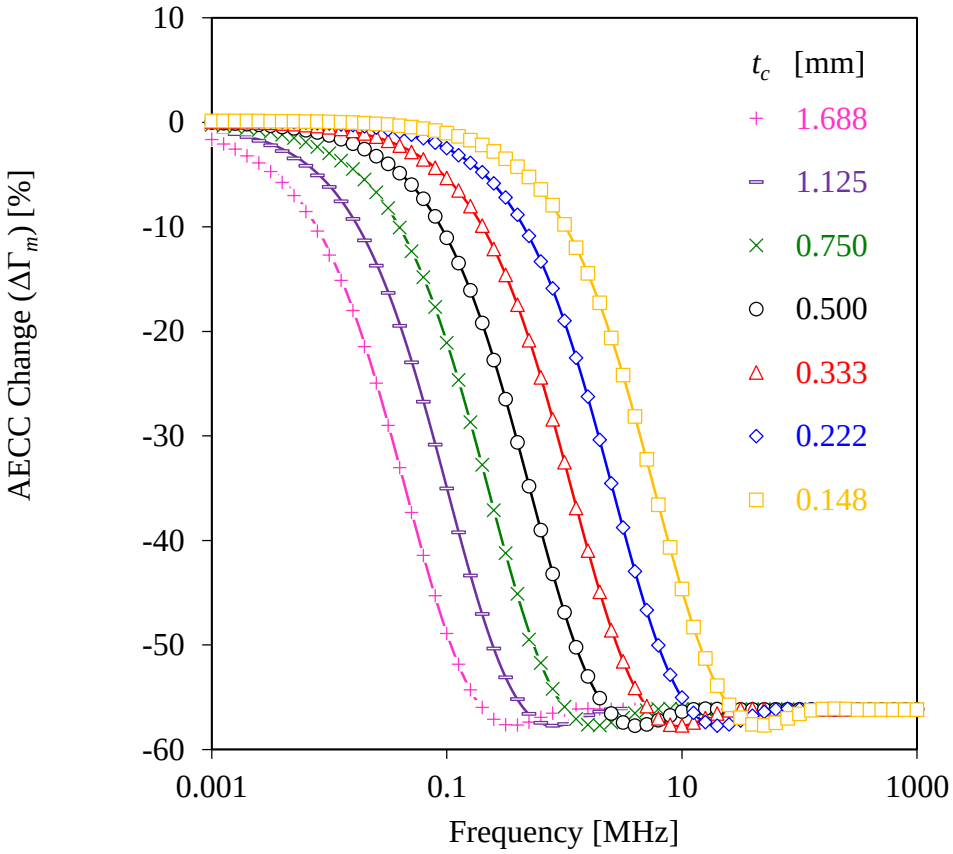

Figure 10. AECC change following the plane-wave approximation (solid lines) and COMSOL simulations (empty markers) on rectangular conductivity profiles of different Ti-6Al-4V coating thicknesses over semi-infinite SS304 substrate [10].

Figure 11(c) illustrates the variation in the coil resistance spectrum due to changes in lift-off where the crossing frequency of the 1Ω line changes with lift-off for the same thickness value of 0.75 mm. This effect is further illustrated in Figure 11(d) where the probe characteristic curve is established at a reference distance of 0 μm for estimating coating thickness. From the figure, it can be seen that there is a significant deviation in the probe characteristic curves for the 3 different lift-off distances. Assuming the probe characteristic curve was established at 25.4 μm lift-off, this allows analyzing the lift-off effect on the impedance-based inversion model uncertainty in a ±25.4 μm lift-off range.

A comparison of the accuracy between the impedance-based and the AECC based method is shown in Figure 12 for estimating coating thicknesses. Since the range of thicknesses is plotted in a logarithmic scale, only thicknesses up to 1 mm were included in the analysis. As expected when compared to the plane-wave approximation which is used to simulate the "measured" AECC change, the spectroscopy AECC based inversion model offers a 0.1% standard deviation from the actual or "input" coating thickness. While using COMSOL to simulate the "measured" AECC spectrum over the coating thicknesses, a 3% standard deviation from the actual or "input" coating thicknesses measured at a lift of range of ±25.4 μm. The main cause of this uncertainty is due to the uncertainties offered in the COMSOL simulations while estimating the "measured" AECC spectrums, which is actually more representative of actual AECC measurement uncertainties. Using the data obtained from Figure 11(d), the impedance-based model offers a 30% uncertainty in estimating coating thicknesses measured at ±25.4 μm lift-off range as shown in Figure 12. For the selected coil design *L* the 1Ω crossing frequency loses its sensitivity to relatively large coating thicknesses. However, as discussed earlier since the eddy current penetration depth becomes more consistent with the standard penetration depth at low frequencies, it is expected that selecting a large coil diameter will result in a 30% uncertainty. Overall the spectroscopy AECC-based model exhibits its robustness to lift-off deviations in estimating coating thicknesses of nonmagnetic metal coating over nonmagnetic metal semi-infinite substrates while offering one order of magnitude improvement in comparison to the impedance-based model.

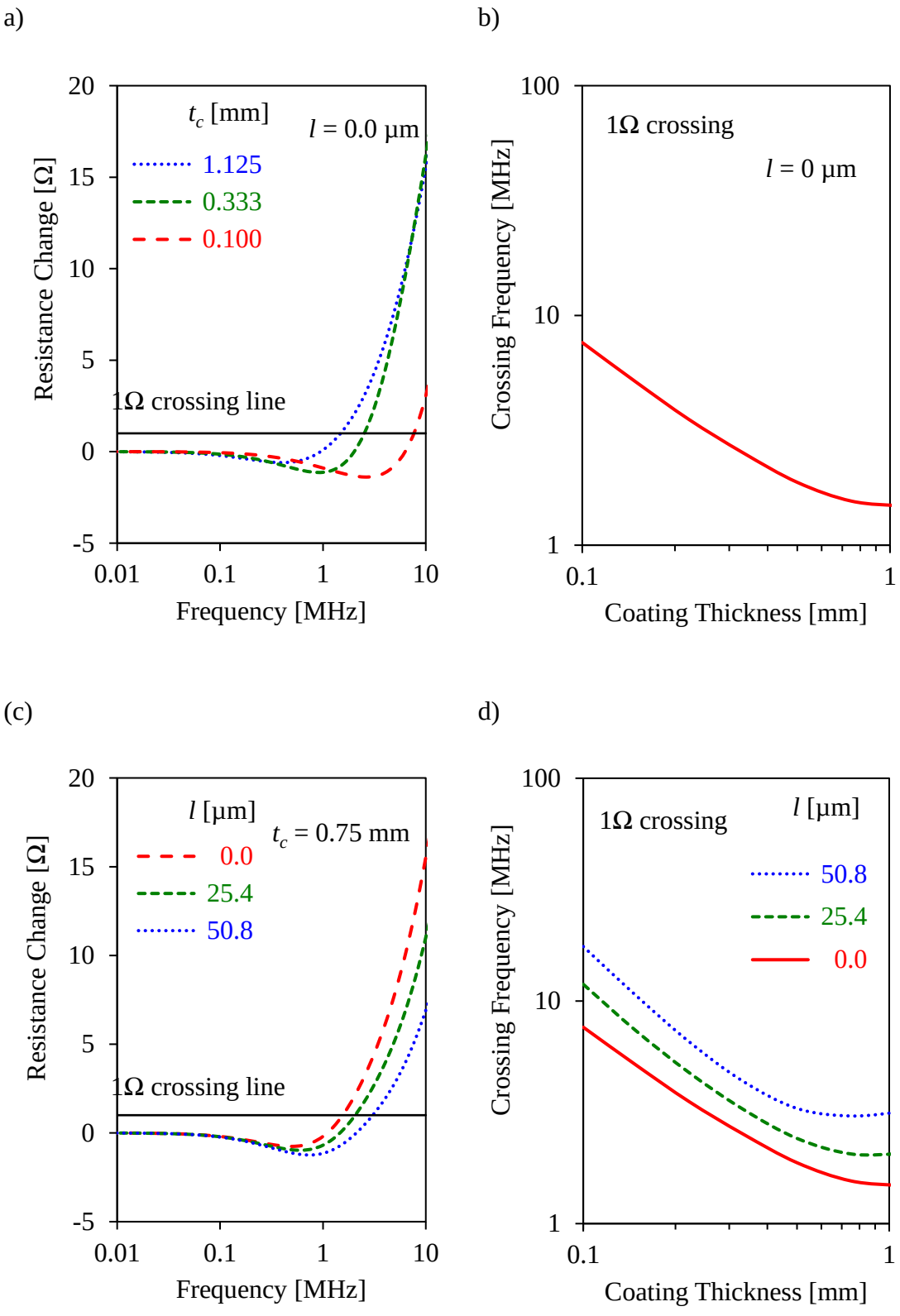

Figure 11. Following the impedance-based method to estimate the coil resistance change spectrum for different coating thicknesses at l = 0.0 µm, for a coating thickness t_c = 0.75mm [10].

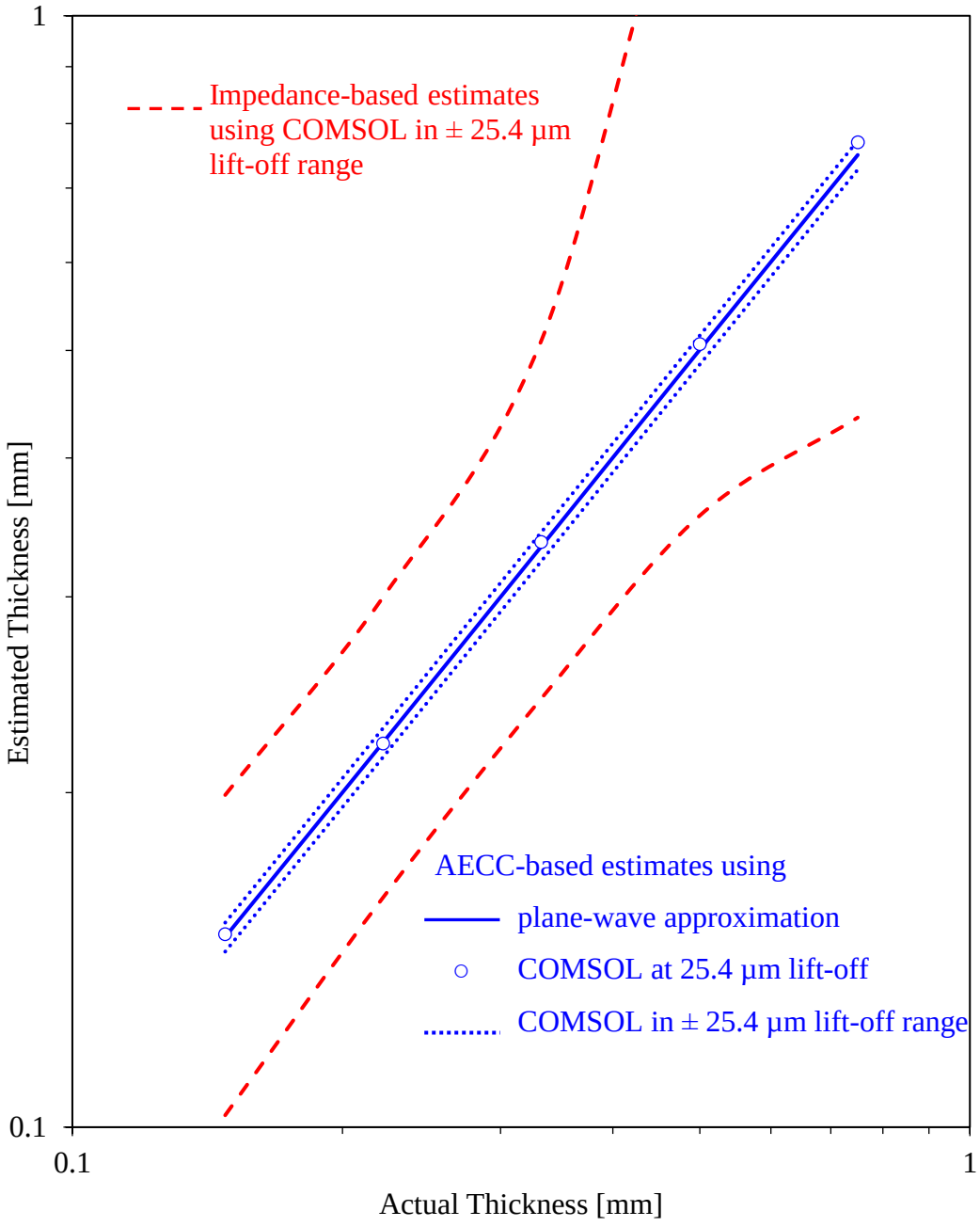

Figure 12. Comparison between the impedance-based and the new AECC-based inversion methods in estimating coating thicknesses [10].

Chapter 3. Single-frequency AECC-based Inversion Model

The spectroscopy AECC-based inversion model proved the feasibility of using AECC to assess metallic coating thicknesses over nonmagnetic metals. However, it brings forward several challenges that need to be addressed at an early technological level before the system can be practically implemented. This chapter will address these challenges and present solutions to overcome them. More importantly, a new AECC-based inversion algorithm is presented to estimate the coating thickness of metallic coating thicknesses over nonmagnetic metals [40].

3.1. Frequency Optimization

AECC spectroscopy has already demonstrated its potential capabilities to assess metallic coating thicknesses over non-magnetic metals [10]. However, it requires a broad inspection frequency to cover, which makes the technique unpractical for industrial applications. The goal of this study is to make AECC measurements more practical by taking AECC measurements at a single frequency. To accomplish this step, it is critical to select an inspection frequency that offers the best sensitivity to assess a coating thickness range of interest. Following the plane-wave approximation, Figure 13(a) shows the AECC change with inspection frequency over a nominal coating thickness of interest, i.e., t_c = 0.5 mm, for the coating/substrate conductivity combination presented earlier using Ti-6Al-4V and SS304, respectively. Figure 13(b) demonstrates the corresponding sensitivity of AECC change to frequency($\partial\Delta\Gamma/\partial f$). This sensitivity analysis indicates that the best sensitivity is offered at an inspection frequency of f = 0.52 MHz for a nominal coating thickness of t_c = 0.5 mm.

This selected frequency needs to be checked against the coating thickness range of interest and whether it offers sufficient sensitivity to cover this range or not. Fine-tuning the inspection frequency to cover this coating thickness range for the coating/substrate conductivity of interest is demonstrated in Figure 14. Following the plane-wave approximation, Figure 14(a) shows the AECC change spectrums for different coating thicknesses. Fine tuning the inspection frequency to cover the coating thickness range of interest, an optimum frequency of f_0 = 0.32 MHz was selected (vertical dashed-line) and displayed along with the AECC change (empty circles) for different coating thicknesses as shown in Figure 14(b). It can be seen that this

frequency gives a unique solution for the AECC change at different coating thicknesses. This is better illustrated in Figure 14(c) for the coating thickness range of interest.

The optimum frequency delivers a balance in AECC change sensitivity to coating thicknesses as presented in Figure 14(d) to cover the coating thickness range of interest in this study between 0.15 and 1.5 mm. The two horizontal dashed-lines in Figure 14(b) represent the upper and lower bounds for the AECC change to be considered in this measurement. Above the upper limit, the AECC change sensitivity is extremely low, which can result in a relatively considerable uncertainty for small coating thicknesses. Below the lower limit, the small "hump" in the AECC change spectrums are overlapping and can result in more than one solution for coating thickness estimation. Any conductivity change measured between the upper and lower bounds will deliver a unique coating thickness estimation at the optimum inspection frequency. It is worth mentioning here that for a given coating/substrate metallic combination, changing the coating thickness range of interest requires changing the optimum inspection frequency (f_0) using the same approach described in this subsection.

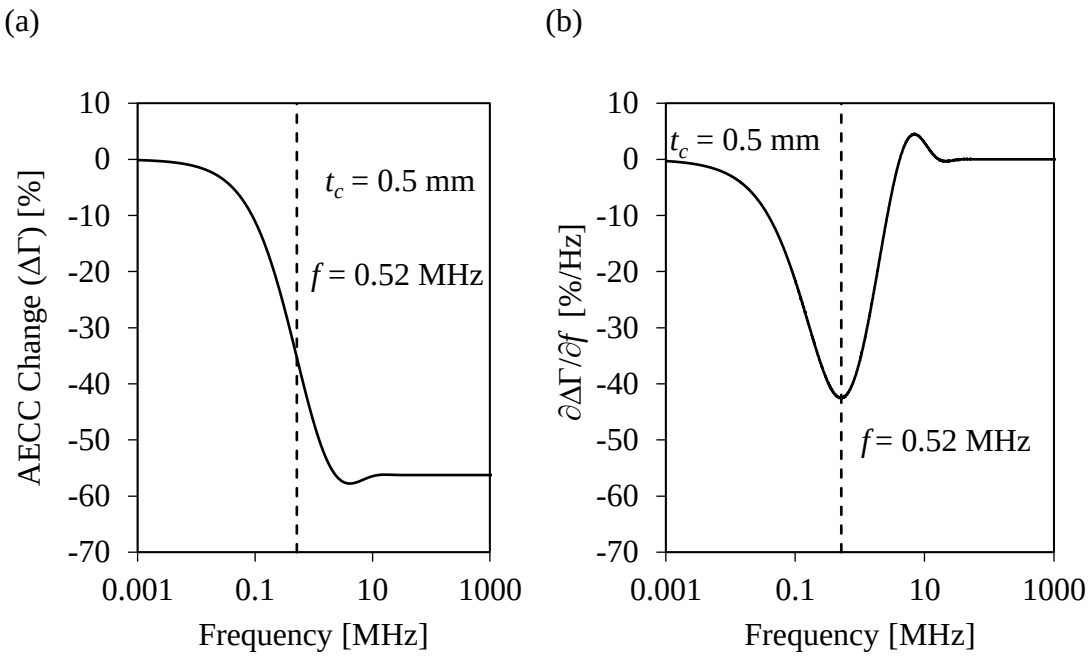

Figure 13. Illustration of AECC change and the sensitivity of AECC change to inspection frequency over a nominal coating thickness of interest, i.e., tc = 0.5 mm, using the plane-wave approximation.

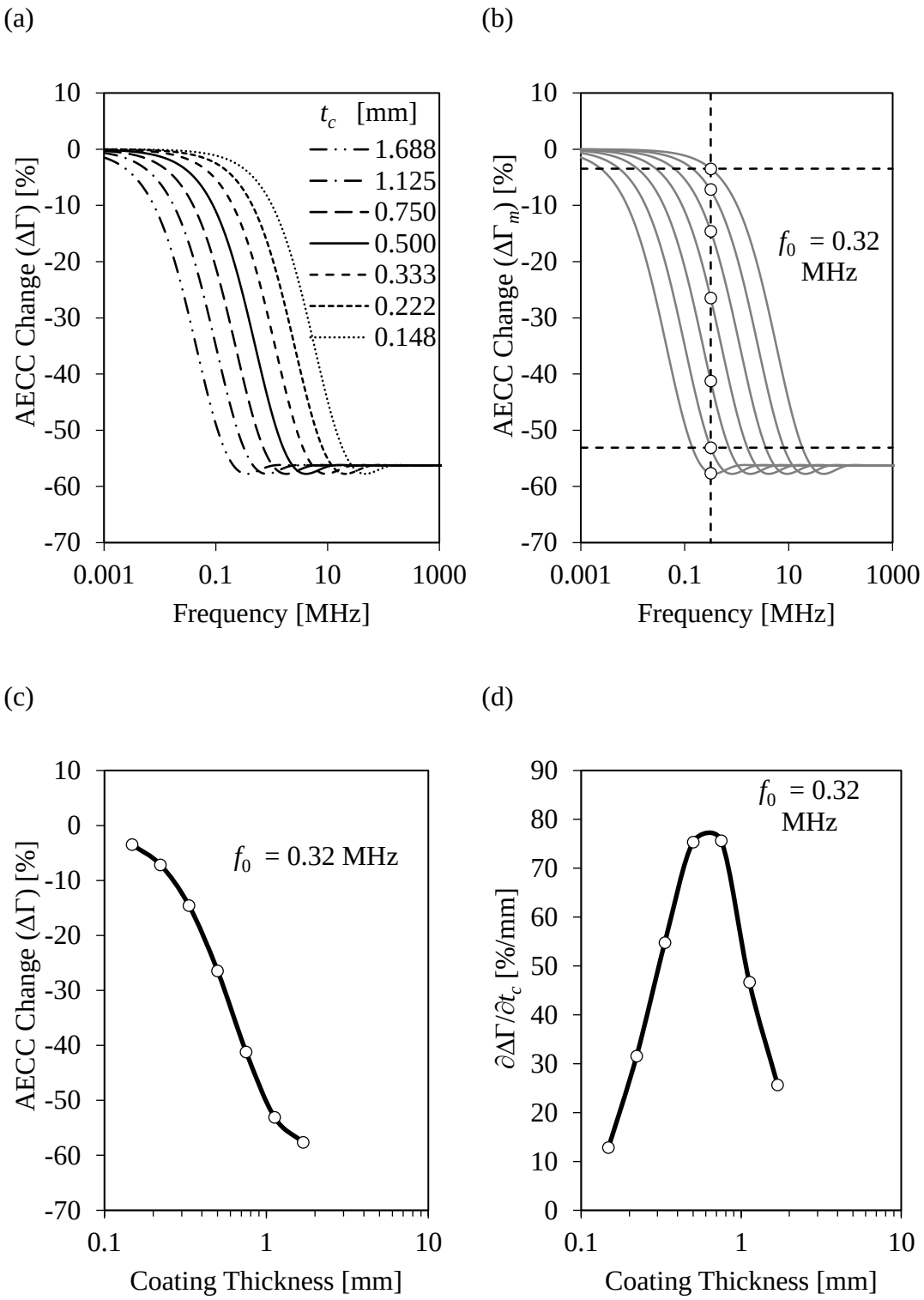

Figure 14. Fine-tuning the inspection frequency based on AECC change sensitivity to coating thickness variations using the plane-wave approximation.

3.2. Coil Selection

So far, AECC measurements require a relatively large coil diameter (D = 50 mm) to meet the plane-wave approximation [10]. This coil design makes this measurement technique unpractical for actual applications, which typically calls for a much smaller diameter. The optimum inspection frequency (f_0 = 0.32 MHz) presented in the previous subsection lends itself for reducing the coil diameter. The capacitive coupling in AECC measurements is minimized since it operates well below 10 MHz. The need for this model to work on semi-infinite substrates is eliminated since the standard eddy current penetration depth at 0.32 MHz is 0.754 mm for SS304 substrates of 2.40 %IACS. Both of these factors allow reducing the coil diameter selection for this measurement.

Figure 15(a) shows COMSOL simulated AECC change ($\Delta\Gamma$) for a range of coil diameters over a nominal coating thickness of 0.5 mm using the same coating/substrate combination. It is clearly seen that selecting a coil diameter less than 16.9 mm results in a deviation from the plane-wave approximation, especially at low frequencies where the standard eddy current penetration depth is not met. To find the minimum coil diameter that meets the plane-wave approximation over a broad frequency range, Figure 15(b) shows the AECC change at 0.001 MHz for different coil diameters. Conducting a best-fit analysis on this data indicates the need for, at least, a 15-mm diameter coil to meet the plane-wave approximation (solid line) as confirmed in Figure 15(c) in close comparison with COMSOL simulations (empty circles).

In general, the 15-mm diameter coil is a practical design in comparison to commercially available eddy current probes and conductivity measurement systems. Further reduction in the coil diameter to as low as 3 mm is illustrated in a later section with the use of a systematic correction factor. Figure 16 illustrates the effect of the coil diameter on AECC spectroscopy for different coating thicknesses using (a) 15-mm, and (b) 3-mm coils. As illustrated in Figure 16(a), COMSOL simulations (markers) of the 15-mm coil shows a slight deviation in AECC from that simulated using the plane-wave approximation (solid lines) especially at low frequencies. This deviation becomes even larger using the 3-mm coil as shown in Figure 16(b). However, the analysis presented in the previous subsection indicates the need to conduct the AECC measurements at 0.32 MHz (vertical dashed-lines) where the deviation is minimized. Due to the

systematic nature of this deviation, the benefits of implementing a correction factor will be illustrated in a later section to reduce the coil diameter to as low as 3 mm.

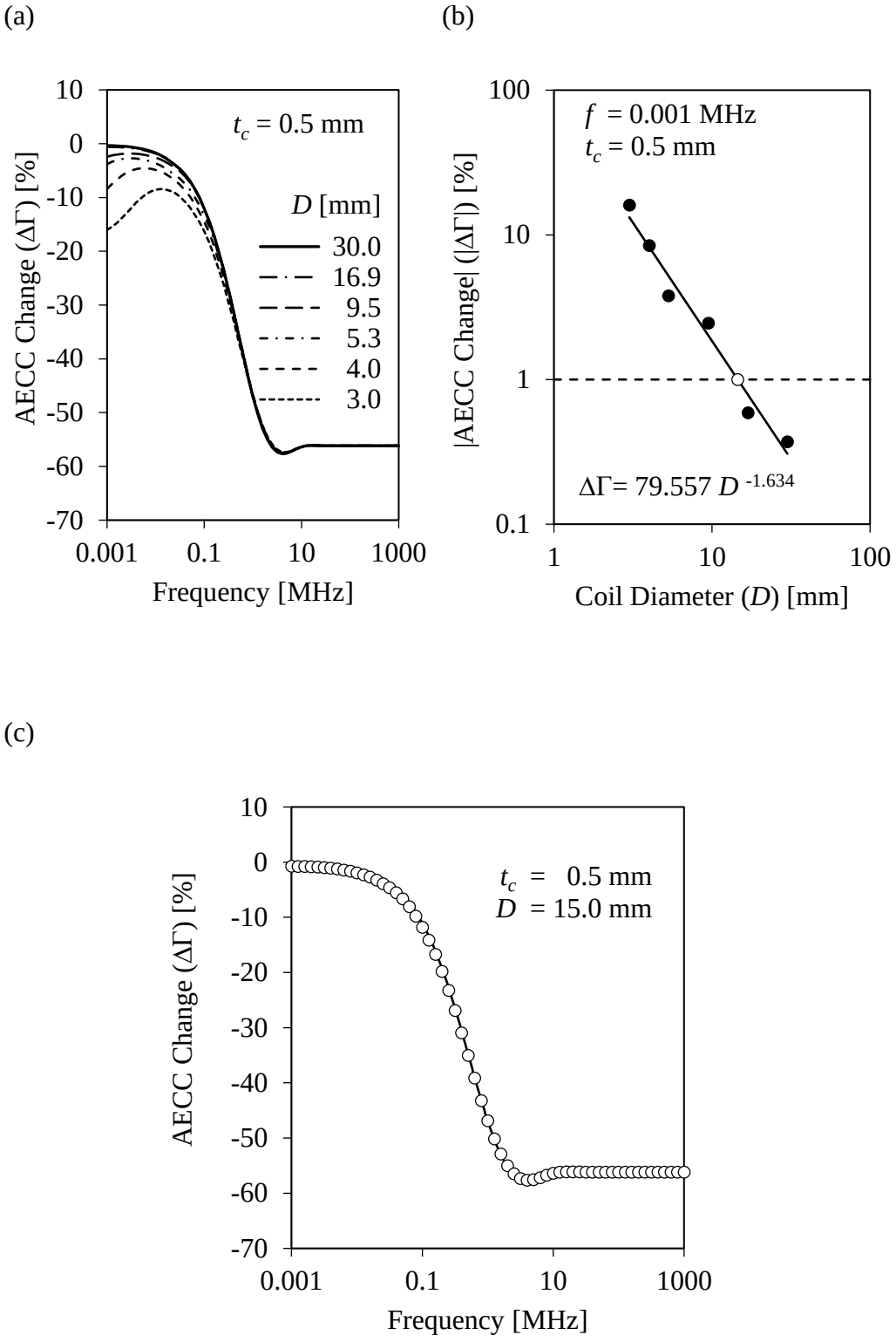

Figure 15. Optimizing the coil design to fulfill the plane-wave approximation over the nominal coating thickness of interest.

(a)

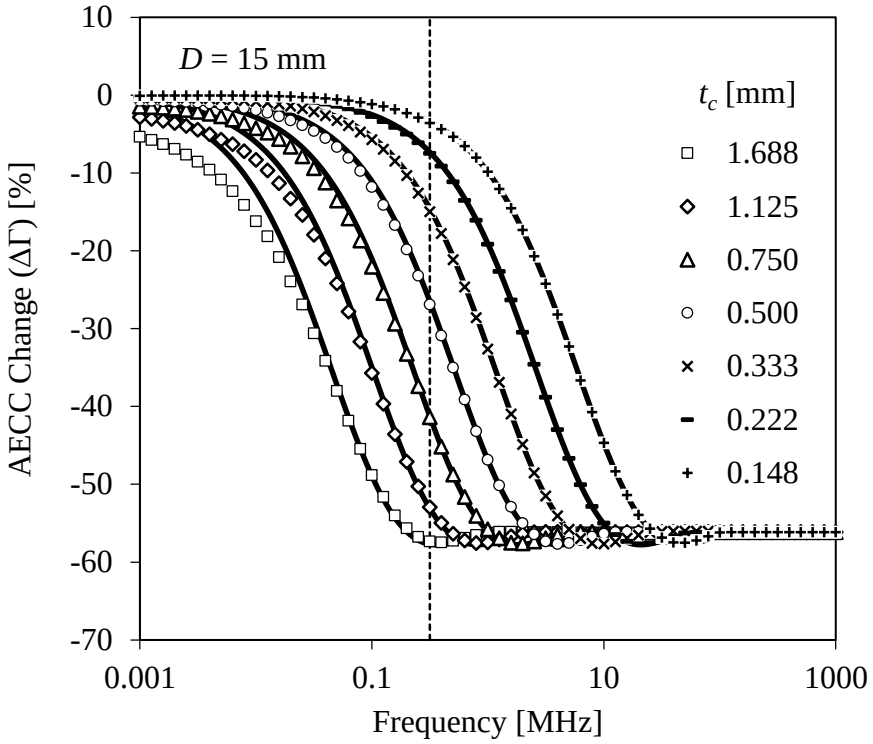

(b)

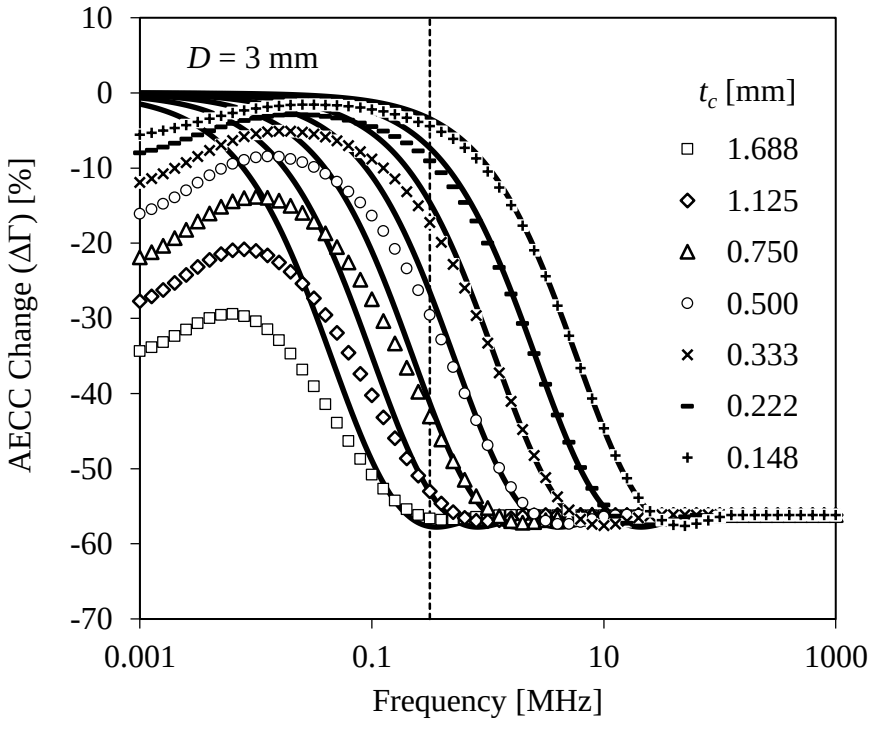

Figure 16. Analysis of the coil design effect on the deviation of AECC change following COMSOL simulations (markers) in comparison to the plane-wave approximation (solid lines) using 15-mm and 3-mm coils.

3.3. Calibration Block Selection

To cover a large range of AECC (≈56%) with accuracy over a broad frequency, range using the indirect approach, more than two calibration blocks are required [10]. For that reason, ten calibration blocks were previously used, which ranged between 1.00 and 2.58 %IACS offering 10.5% variations between any two consecutive calibration blocks. However, in single-frequency AECC measurements spot measurements, only two consecutive calibration blocks are needed with conductivity values bracketing the AECC value of interest. It is worth mentioning here that commercial conductivity meters, such as SigmaCheck-2 Eddy Current Conductivity Meter, offer ±0.05 %IACS uncertainty in 0-20 %IACS and 0.5 mm lift-off range at a single frequency. With slight modification to a calibrated conductivity meter, the selection of the calibration blocks can be eliminated.

3.4. Proposed Single-frequency AECC-based Inversion Algorithm

The introduction of the recent spectroscopy AECC-based model [10] extended the capabilities of AECC spectroscopy to estimate metallic coating thicknesses over nonmagnetic metals. However, it mandates measuring the AECC spectrum over a broad frequency range, which makes the measurement technique rather unpractical. With the use of the proposed single-frequency AECC coating thickness assessment of depth-dependent rectangular conductivity profiles, a new AECC-based inverse model is needed. To build the new inverse model, the rectangular conductivity profile shown in Figure 2(a) is used to simulate Ti-6Al-4V (σ_c = 1.05 %IACS) coating over SS304 (σ_s = 2.40 %IACS) semi-infinite substrate where the coating thickness is relatively small in comparison to the sample's overall thickness. The coating thickness t_c used here is 0.5 mm and the selected numerical interpolation method is the bisection method since a single AECC measurement is used.

The proposed flow diagram for the new AECC-based inverse algorithm is illustrated in Figure 17. To start the process, the measured AECC change $\Delta\Gamma_m$ at the selected frequency f_0 along with the initial guesses of coating thicknesses t_0 and t_1 are defined by the upper and lower control limits to cover the thickness range of interest. Then a tolerance level ϵ is specified as the accepted criterion for the iterations to pass through. The conductivities of coating and substrate materials are assumed to be known or measured separately, which is consistent with existing impedance-based and AECC-

based inversion models [4, 7]. Starting with the first iteration (n = 1), $\Delta\Gamma_{n-1}$ and $\Delta\Gamma_n$ at the selected frequency f_0 are estimated for coating thicknesses t_{n-1} and t_n using the plane-wave approximation. As previously illustrated, the 15-mm coil design delivers AECC measurements in agreement with the plane-wave approximation at the selected frequency. This further exploits the plane-wave approximation for the proposed AECC-based inversion model. A new estimated thickness t_{n+1} is introduced following the bisection method as follows:

$$t_{n+1} = 10^{\frac{\log_{10} t_{n-1} + \log_{10} t_n}{2}}, \tag{6}$$

due to the logarithmic nature of the problem. Taking this new thickness value, the corresponding AECC change $\Delta\Gamma_{n+1}$ is estimated at f_0 again using the plane-wave approximation. The difference between the measured AECC change ($\Delta\Gamma_m$) with both $\Delta\Gamma_{n-1}$ and $\Delta\Gamma_{n+1}$ are taken and multiplied with each other. If the product yields a negative value, then t_{n+1} and $\Delta\Gamma_{n+1}$ replace t_n and $\Delta\Gamma_n$ respectively to proceed further with the algorithm. If the product yields a positive value, then t_{n+1} and $\Delta\Gamma_{n+1}$ replace t_{n-1} and $\Delta\Gamma_{n-1}$ respectively. This process is repeated until the absolute difference between the measured AECC change $\Delta\Gamma_m$ and the simulated AECC change $\Delta\Gamma_{n+1}$ using the plane-wave approximation reaches acceptance tolerance criteria. The next section discusses the accuracy of the proposed algorithm as well as the further reduction of the coil diameter with the use of a systematic correction factor. Moreover, it also compares thickness estimates using the impedance-based method against the proposed single-frequency AECC-based model with the reduced coil diameter.

3.5. Accuracy of the New AECC-based Inversion Algorithm

This section demonstrates the convergence of the proposed single-frequency AECC-based inverse model using the coating/substrate combination illustrated in Figure 2(a), and will further be extended for different coating thicknesses using different coil diameters. Moreover, the performance of the proposed AECC-based model is compared with the existing impedance-based one for a relatively small coil diameter. Using a 15-mm diameter coil, which meets the plane-wave approximation at the selected frequency of f_0 = 0.32 MHz, delivers a "measured" or simulated AECC change of $\Delta\Gamma_m$ = -26.90% over 0.5-mm coating thickness as shown in Figure 16(a). To start the proposed inverse model, initial thickness values of t_0 = 0.1 mm and t_1 = 1.1 mm were selected as well as a tolerance limit of $\epsilon = 1\text{x}10^{-5}$ was specified. Figure 18(a)

shows the convergence of the estimated AECC change using the 15-mm diameter coil at a frequency of 0.32 MHz.

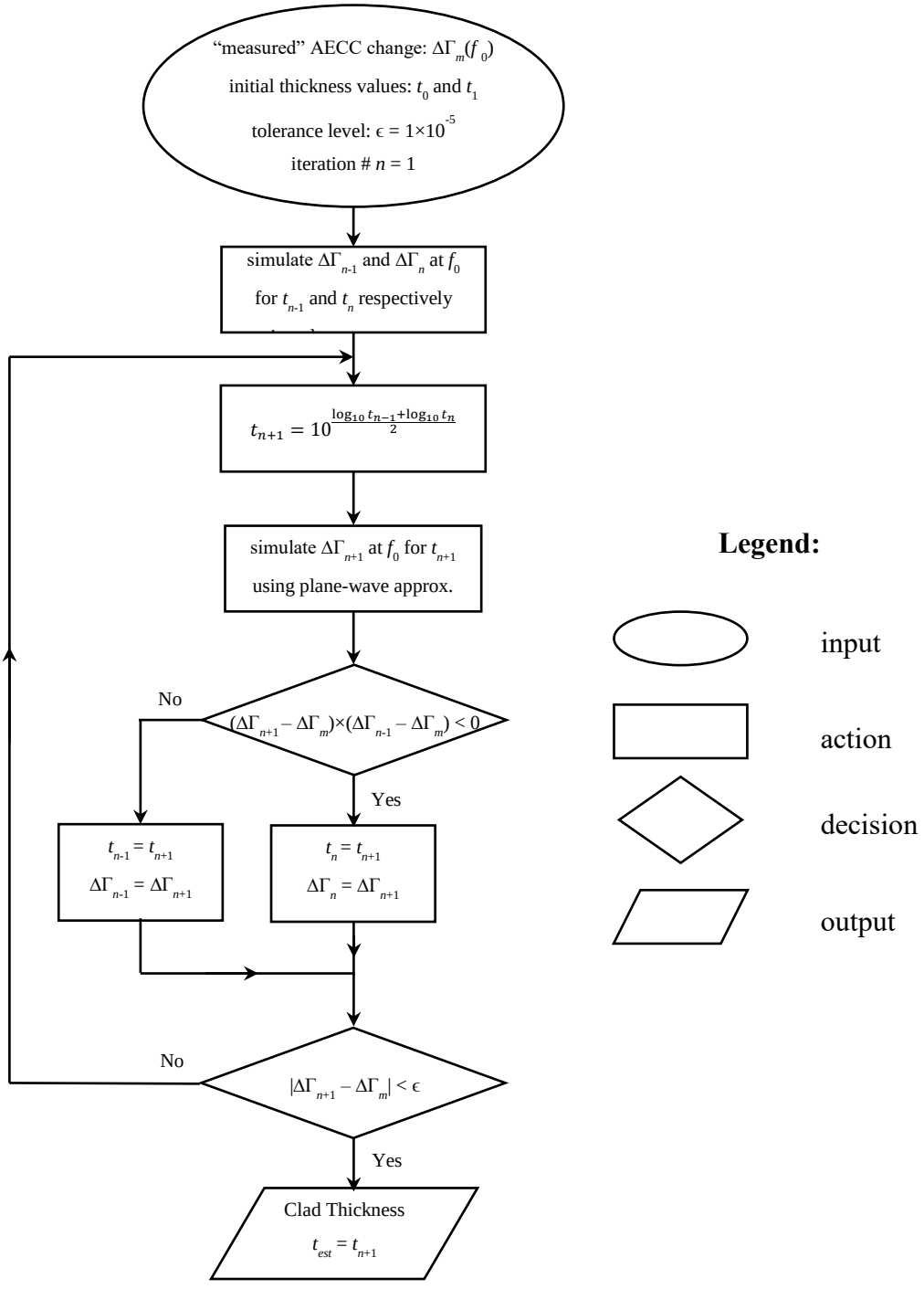

Figure 17. A flow diagram of the proposed single-frequency AECC-based inversion algorithm to estimate metallic coating thicknesses over nonmagnetic metals using the Bisection method.

It takes about 10 iterations for the AECC change $\Delta\Gamma_n$ to converge to the measured one $\Delta\Gamma$m = -26.90%. The corresponding convergence of coating thicknesses t_n to the estimated coating thickness test = 0.505 mm is demonstrated in Figure 18(b). It slightly over estimates the actual coating thickness (≈ 1% over estimation) due to the reduced coil size. A similar analysis is presented in Figure 18(c) using a 3-mm diameter coil where AECC change $\Delta\Gamma_n$ certainly converges to the measured one $\Delta\Gamma_m$ = -29.51% taken from Figure 16(b). However, it delivers an estimated coating thickness of t_{est} = 0.543 mm since the measured AECC change corresponds to an equivalent coating thickness using the plane-wave approximation. This systematic over estimation of ≈ 8.6% is mainly due to the use of a very small coil diameter.

In comparison to actual coating thicknesses, Figure 19(a) shows the corresponding coating thickness estimates measured at 0.32 MHz with 25.4 μm lift-off using different coil diameters. Analyzing this data clearly indicates the systematic nature of this error as a function of coil diameter. It simply shows that decreasing the coil diameter deviates AECC measurements from the plane-wave approximation. This systematic error can be easily corrected for using best-fit analysis as follows:

$$t_{est} = a{t_{est^*}}^b, \tag{7}$$

where t_{est} is the estimated coating thickness from the proposed single-frequency AECC-based model and t_{est^*} is the corrected coating thickness estimate. The constants *a* and *b* are estimated once and for all using the best-fit analysis for a given coil design and coating/substrate conductivity combination. Accordingly, t_{est^*} can be evaluated by rearranging the above equation as follows:

$$t_{est^*} = \left(\frac{t_{est}}{a}\right)^{\frac{1}{b}}. \tag{8}$$

Using the latter equation, corrected coating thickness estimates show an agreement with actual coating thicknesses as illustrated in Figure 19(b) regardless of the coil diameter.

Applying the correction factors shown in Table 1, which capture to systematic nature of measurement deviations, allow reducing the coil diameter to as low as 3 mm. If the coil diameter meets the plane-wave approximation at the optimized frequency for a coating/substrate combination, i.e., $D \geq 15$ mm in this study, then there is no need to

Table 1. Correction factors to reduce the systematic error encountered while reducing the coil diameter.

Coil Diameter [mm]	**a**	**b**
3.0	1.0221	0.9367
4.0	0.9996	0.9552
5.3	0.9917	0.9694
9.5	0.998	0.9827
15.0	0.9983	0.9903
50.0	0.9992	1.0023

apply any corrections. The use of smaller coil diameters requires applying these corrections. Since the measurement is required at a single frequency, commercially available eddy-current-based conductivity meters can be easily leveraged for this application. Tabulating the measurement correction constants *a* and *b* associated with a given coil diameter to be used over a specific coating/substrate combination to cover a predefined coating thickness range at an optimized inspection frequency allows inverting the measured AECC to the corrected estimated thickness in Eq. (8). Figure 20 further illustrates the robustness of the proposed model, where coating thickness estimation is simulated following both multi-frequency impedance-based model [7] and the proposed single-frequency AECC-based model with a 3mm coil in a ±25.4 μm lift-off range. Detailed analysis of the multi-frequency impedance-based model can also be found in a recent study demonstrating its capabilities against the multi-frequency AECC-based model [10]. As expected, using the plane wave approximation delivers negligible deviation (≈ 0.1%) in estimating coating thicknesses. Using COMSOL, the corrected thickness estimates using a 3-mm diameter coil delivers an average of 3% variations in a ±25.4 μm lift-off range. This shows an excellent agreement with the previously introduced multi-frequency AECC model which used a much larger coil diameter (D = 50 mm) [10]. Following the impedance model using the 3-mm diameter coil in a ±25.4 μm lift-off range, the impedance-based model delivers 30% uncertainty in coating thickness estimation. For coating thicknesses higher than 0.5 mm, the impedance-based model loses its sensitivity since the coil diameter is rather small to meet the standard eddy current penetration depth. This further strengthens the use of the proposed algorithm as a more efficient technique for coating thickness estimation.

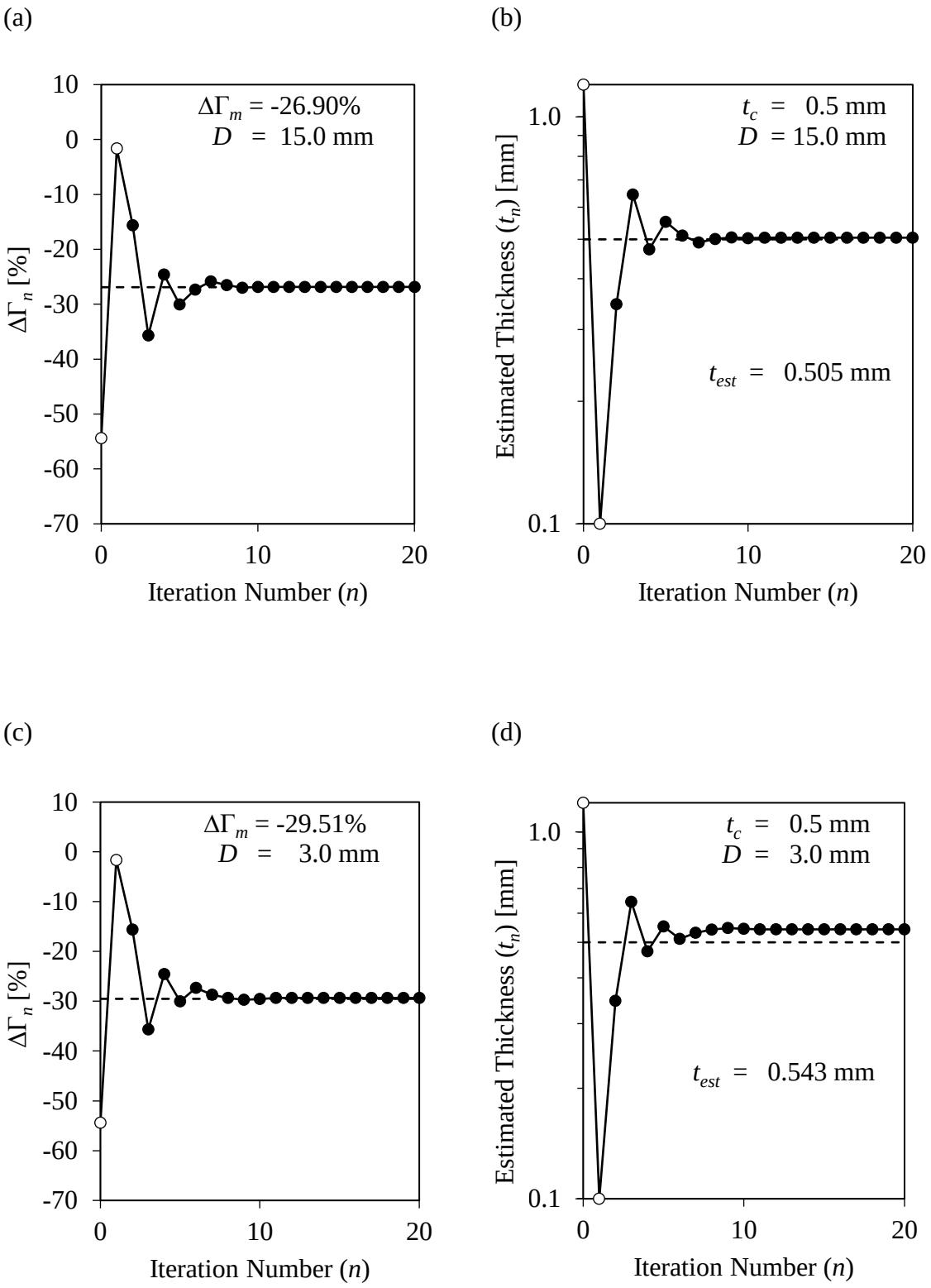

Figure 18. The convergence of estimated AECC change ($\Delta\Gamma_n$) to the measured one and its estimated coating thickness (t_n) at different iterations using 15-mm and 3-mm coils operating at f_0 = 0.32 MHz.

a)

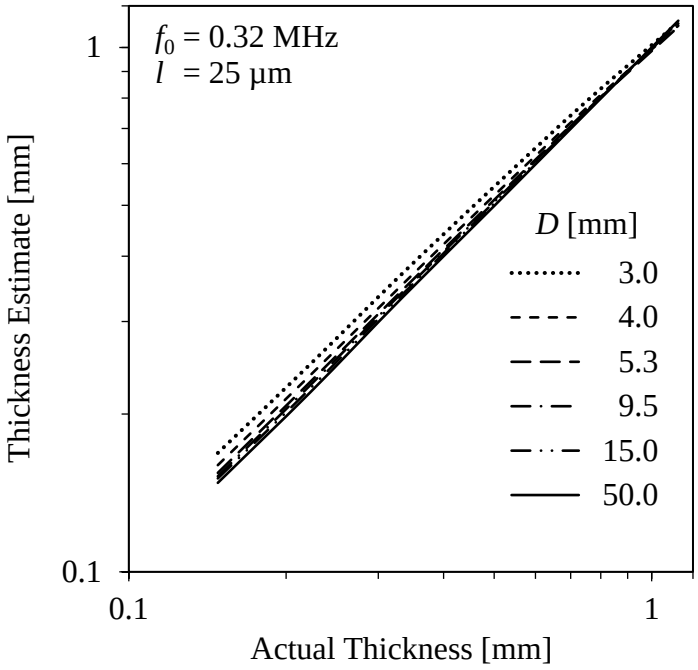

b)

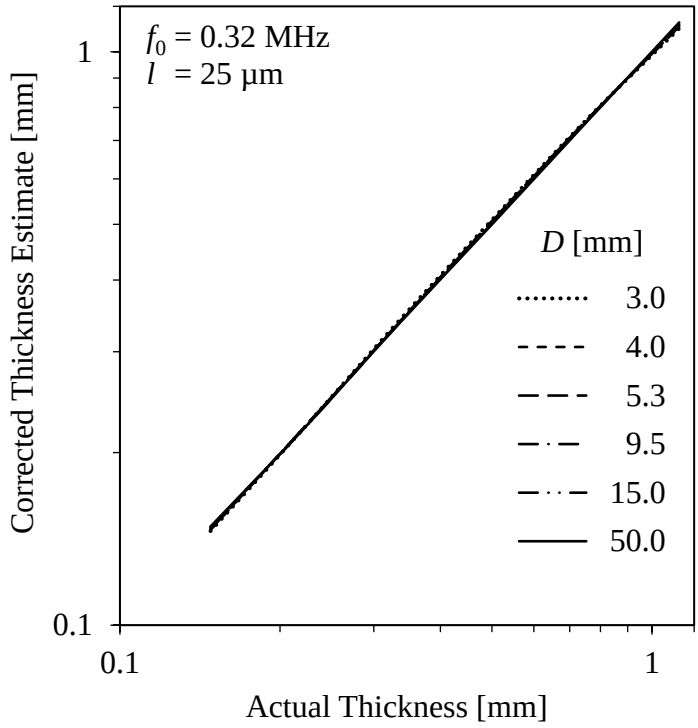

Figure 19. Coil design effect before and after the implementation of systematic correction factors on coating thickness estimation using the proposed single-frequency AECC-based model at 25-µm lift-off distance.

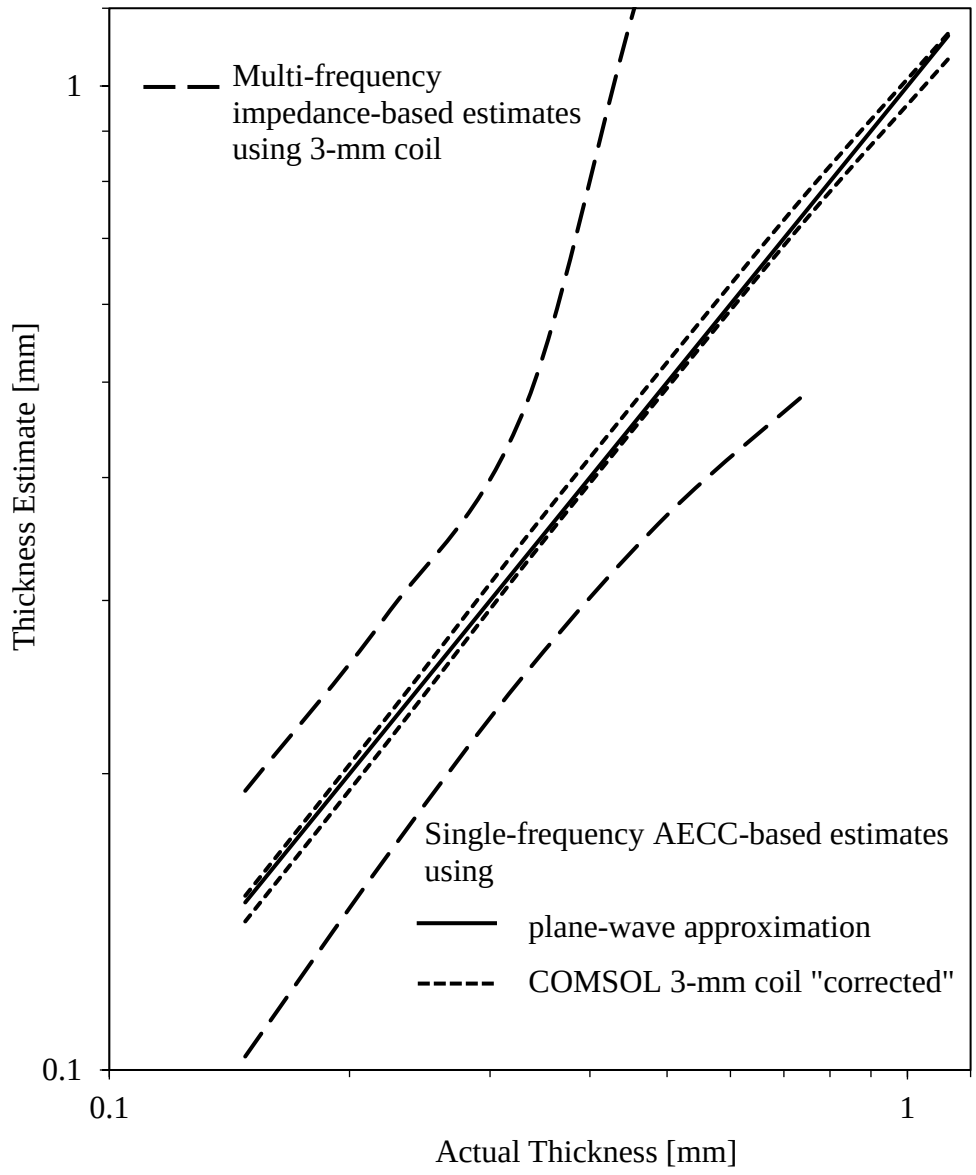

Figure 20. Comparison between the multi-frequency impedance-based model and the proposed single-frequency AECC-based model in estimating coating thicknesses using a 3-mm coil in a ±25.4 μm lift-off range.

Chapter 4. Experimental Validation

With both the AECC inversion models being validated through numerical means, the objective now was to develop a practical system that would be able to evaluate the AECC change for a given coating/substrate combination at any given frequency. For the experimental case, the coating substrate combination was Al 1230 coating over Al 2024 substrate as shown in Figure 21. This type of coating is used to protect the aluminum alloy from corrosion [41]. Since the coating/substrate combination and the coating thickness range of interest have changed, the analysis done in the previous chapter has to be repeated. Furthermore, to maintain consistency with the experimental work, a frequency range of 0.1-15 MHz was used for the COMSOL simulations.

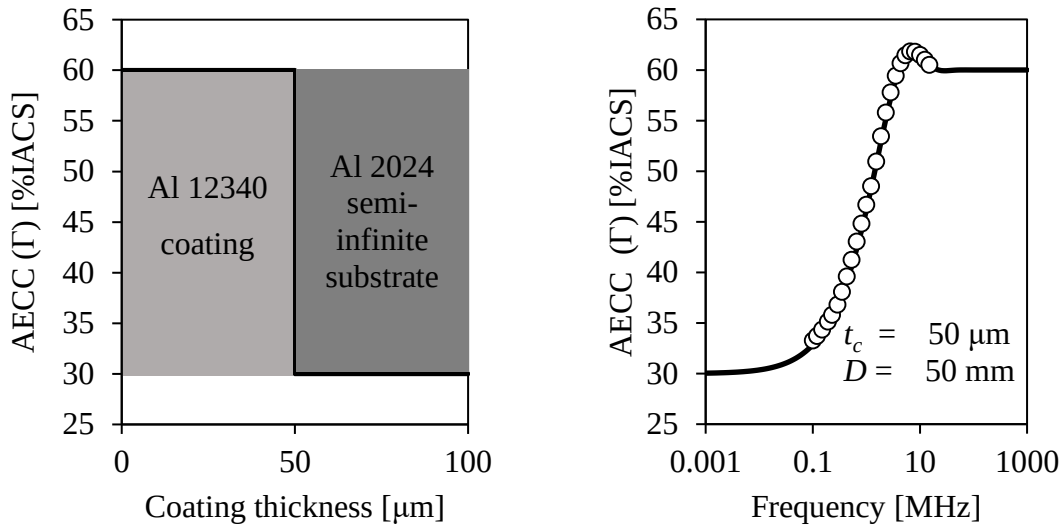

Figure 21. Al 1230 coating over a semi-infinite Al 2024 substrate with a coating thickness of 50 μm rectangular conductivity change and its corresponding AECC change using the plane-wave approximation (solid line) and COMSOL simulations

4.1. Frequency Optimization

Prior to conducting experiments, the given coating substrate combination was simulated on COMSOL with the coating and substrate conductivities being σ_c = 60 %IACS and σ_s = 30 %IACS respectively. Figure 22(a) shows the AECC spectrum for the entire coating thickness range of interest using the plane-wave approximation. Fine tuning the inspection frequency gives a value f_0 = 0.6 MHz as shown in Figure 22(b). From the figure, it can be observed that the selected frequency offers a unique solution for each of the coating thicknesses. This is better demonstrated

in Figure 22(c), where coating thicknesses are plotted against their respective AECC changes at the selected frequency. The horizontal dashed lines shown in Figure 22(b) represent the upper and lower bounds for the AECC change that need to be considered for the measurement. Once again if the AECC value is above the upper limit, the AECC change sensitivity is extremely low which could result in large uncertainties in coating thickness estimation. Below the lower limit the "hump" in the AECC change spectrums are overlapping which will result in multiple solutions for the same coating thickness. Any value between these two limits will result in a unique solution for the coating thickness. Figure 22(d) shows that the selected frequency offers a balance in the sensitivity AECC change to the coating thickness.

4.2. Coil Reduction

Previously a large coil diameter (D = 50 mm) was required to meet the plane wave approximation [10]. This was another challenge that needed to be addressed as commercially available probes are much smaller. Since measurements are now being taken at a single optimum frequency, the coil diameter can be reduced. Following a similar analysis to the one done in the previous chapter, Figure 23(a) shows the AECC change ($\Delta\Gamma$) using different coil diameters for a nominal coating thickness of 50 μm for the same coating/substrate combination. Unlike the previous chapter, the coating and substrate conductivities used in this study is relatively higher to the ones used in that one which has resulted in very low variation in AECC change when the coil diameter is reduced. This is better presented in Figure 23(b) where the AECC change is taken at 0.1 MHz for all the coil diameters. It can be seen that a reduction in coil diameter does not significantly impact the AECC change ($\Delta\Gamma$). Taking advantage of this fact, Figure 23(c) shows the AECC spectrum using the plane-wave approximation (solid lines) as well as COMSOL simulations (empty markers). As expected, the COMSOL simulations are in agreement with the plane-wave approximation even for coil diameter of as low as 3 mm. This is better illustrated in Figure 24, where the AECC change is simulated for a coating thickness range of interest using (a) 50 mm and (b) 3 mm coils. It can be seen that both coil diameters are in agreement with each other with minor deviations.

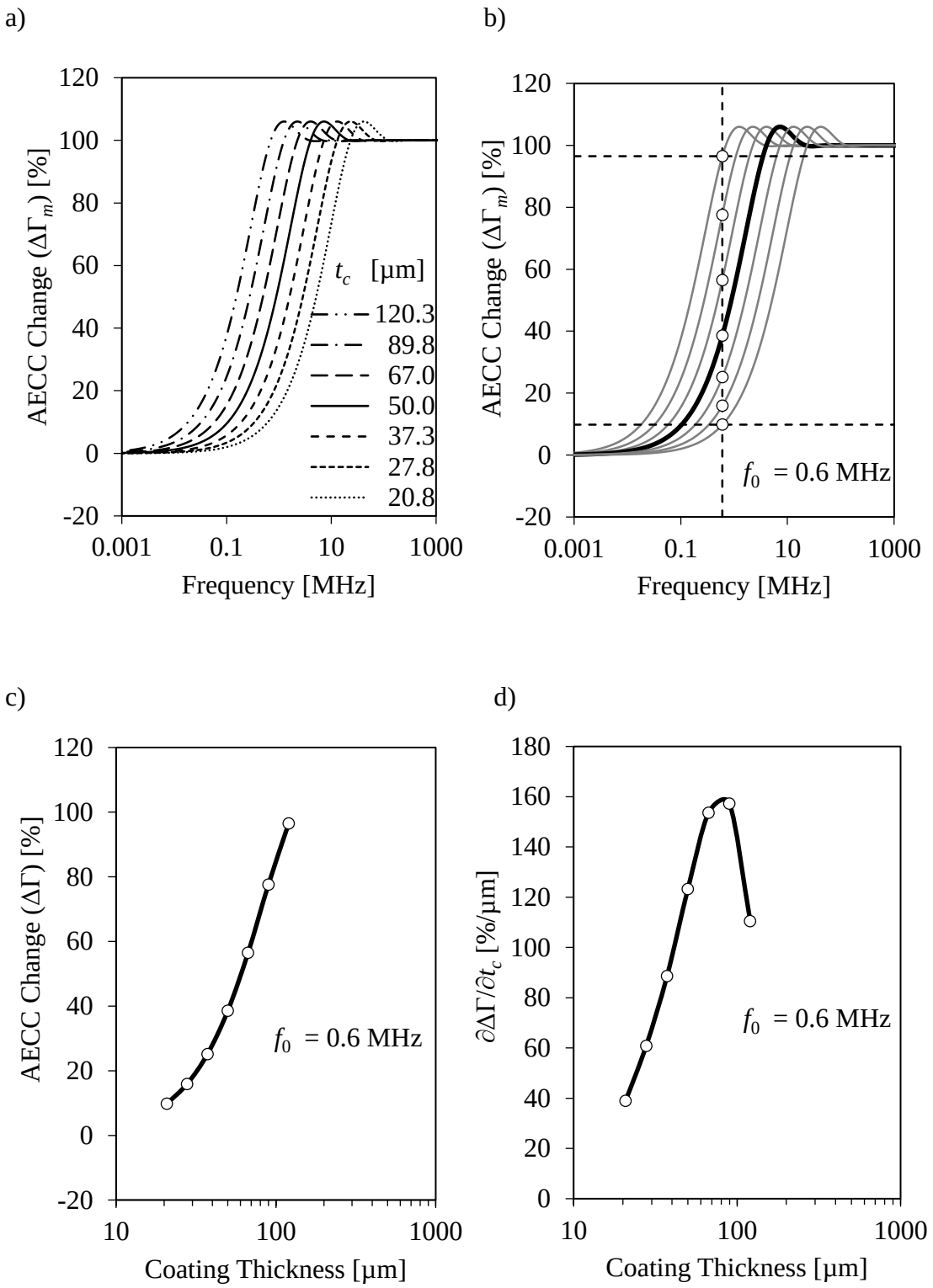

Figure 22. Fine tuning the inspection frequency based on AECC sensitivity to coating thickness variations using the plane-wave approximation

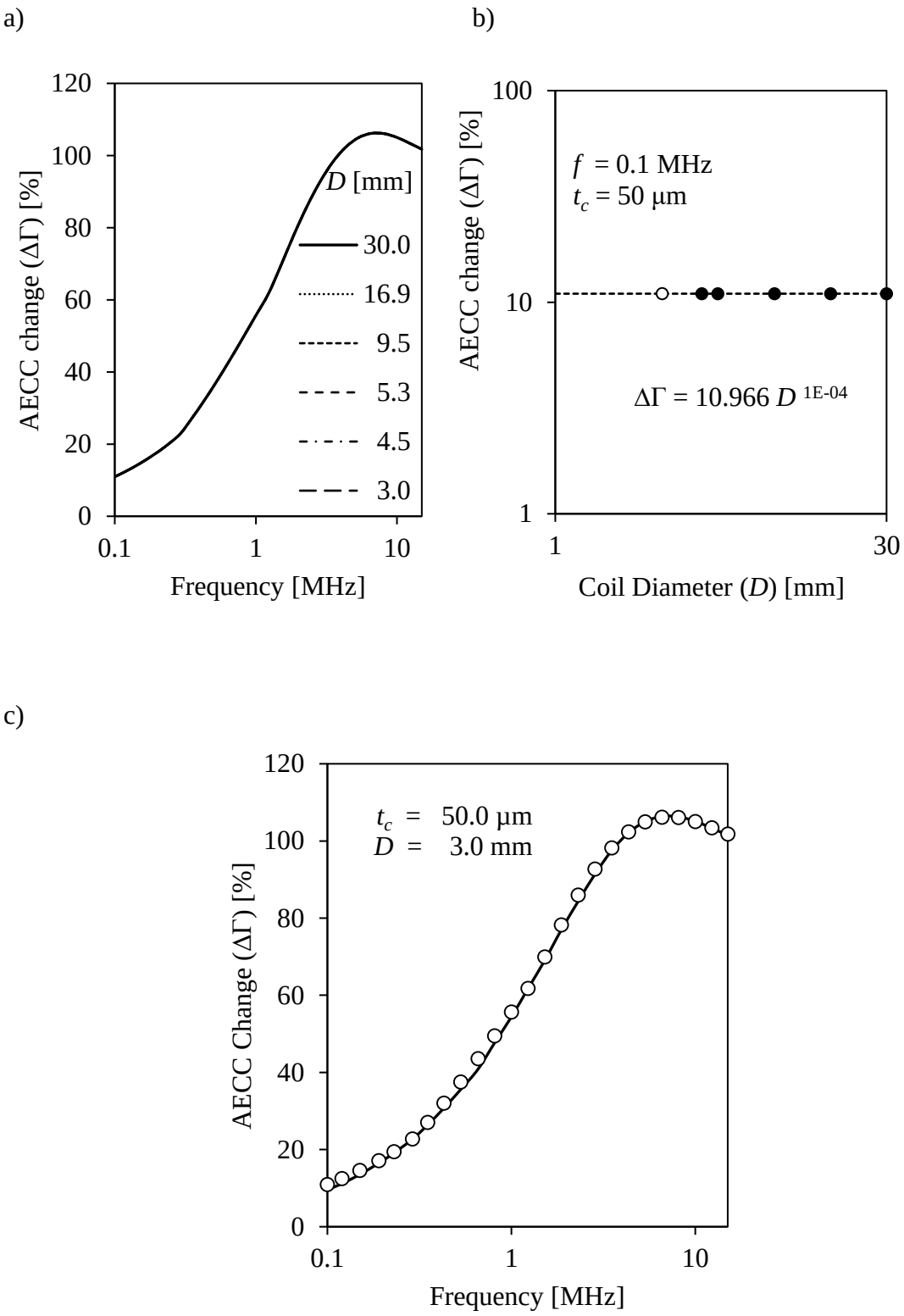

Figure 23. Optimizing the coil design to fulfill the plane-wave approximation over the nominal coating thickness of interest.

a)

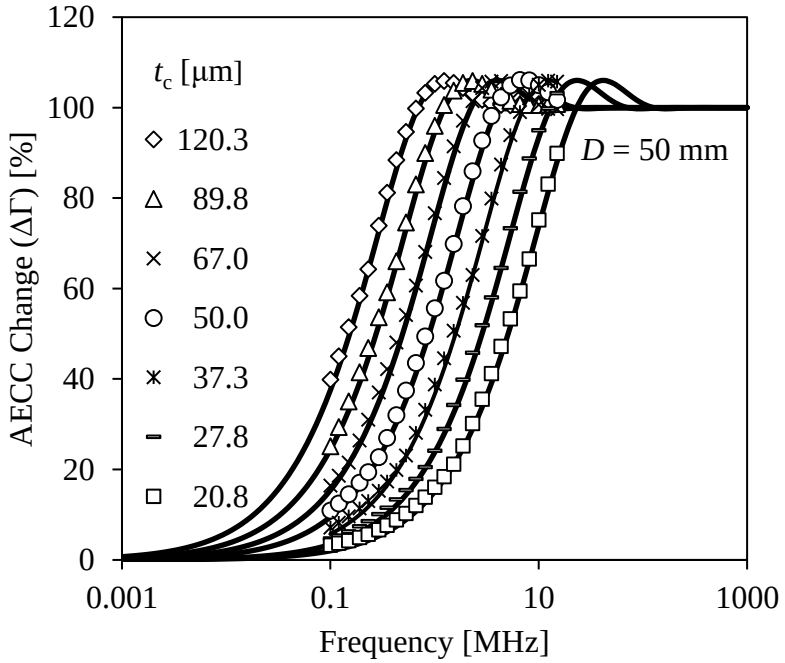

b)

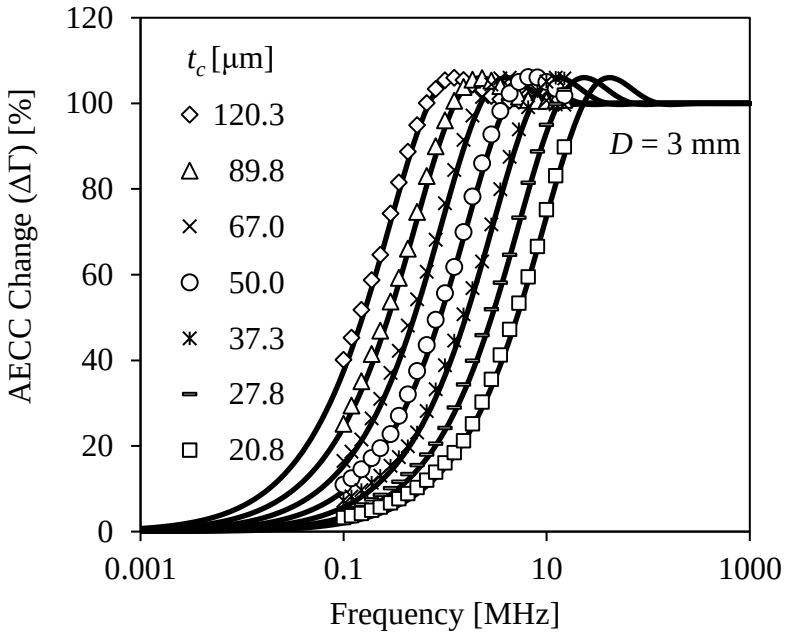

Figure 24. AECC change for Al 1230 coating over Al 2024 substrate at different coating thicknesses following COMSOL simulations (empty markers) using 50-mm and 3-mm coils in comparison to the plane-wave approximation (solid lines).

4.3. Calibration Block Selection

Four calibration blocks were used to cover the entire conductivity range for both the simulation and experimental measurements. For the experiments, the calibration blocks of values 27.98 and 36.65 %IACS were cylindrical in shape with a diameter of 36mm and a height of 11 mm. The third calibration block which had a value of 49.04 %IACS had a rectangular cross section with the length and width being 34 and 25 mm respectively and the height was 6 mm. Finally, the calibration block with the highest conductivity value of 61.65 %IACS was also cylindrical like the first two, with a diameter of 25 mm and a height of 8mm. These calibration blocks were established independently at 120, 240 and 480 kHz frequencies using the commercially available SigmaCheck-2 Eddy Current Conductivity Meter.

4.4. Simulation Results

After obtaining the AECC values for the entire frequency spectrum using COMSOL a comparative analysis is done to evaluate their accuracies in coating thickness estimation. A conductivity value of σ_c = 60 %IACS for the coating and σ_s = 30 %IACS for the substrate was provided to the algorithms. To initiate the iterative process, thickness values t_0 and t_1 were set to be 10 and 130μm respectively. These two values were specified such that they cover the entire coating thickness range of interest. A tolerance limit of $\epsilon = 1x10^{-5}$ was specified as a criterion for convergence.

4.4.1. Spectroscopy results. For the spectroscopy model the AECC spectrum shown in Figure 21(a) was used as the "measured" AECC change. After providing the necessary inputs the inversion algorithm is initiated. Figure 25(a) and (b) shows the convergence of the simulated AECC spectrum with the measured one and the corresponding estimated thickness respectively. It can be seen that the algorithm slightly overshoots the actual coating thickness value with the percentage error being 3.6%. Looking at the coating thickness estimates in Figure 26(a) for the entire coating thickness range, it can be seen that the error is systematic in nature. Repeating the best fit analysis done in the previous chapter, Figure 26(b) shows the coating thickness estimates after applying the corrections. The grey line in the graphs is there as a reference to illustrate the deviation between the estimated and actual coating thicknesses.

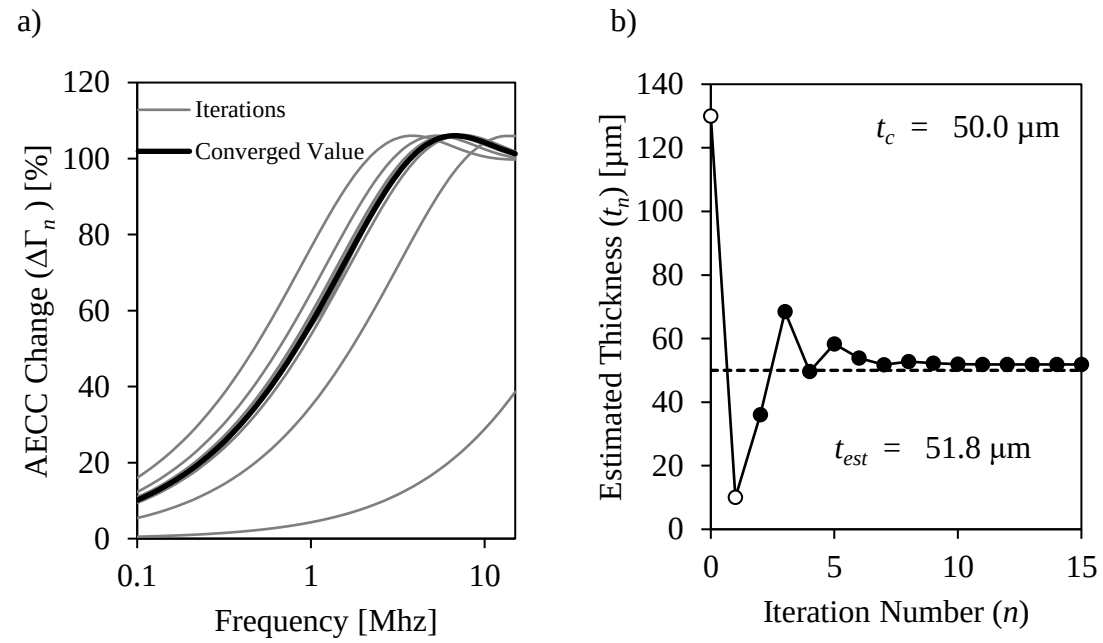

Figure 25. Simulated AECC change ($\Delta\Gamma_n$) iterations (grey lines) converging to the "measured" one (black line) and its corresponding coating thickness estimate using the spectroscopy model.

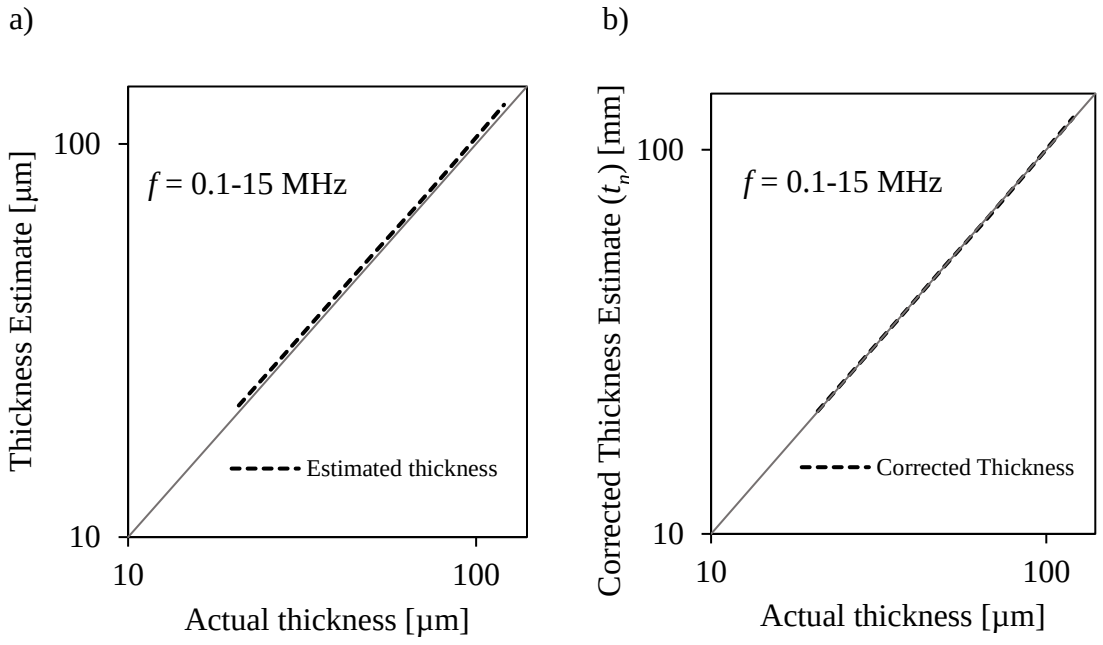

Figure 26. Coating thickness estimates for the entire coating thickness range of interest. Before and after applying a correction factor for the spectroscopy inversion model

4.4.2. Single-frequency results. Moving on to the single-frequency inversion model, Figure 27 shows the convergence of the "simulated" AECC change to the "measured" one and its corresponding coating thickness estimate. Once again the algorithm slightly overshoots the thickness estimate with a slightly higher error percentage (4.4%) when compared to the spectroscopy model. Following the same procedure done for the spectroscopy model, a correction factor is applied here to increase the accuracy in coating thickness estimation. This is shown in Figure 28 after applying the correction factors, both models provide similar estimates for the coating thickness values.

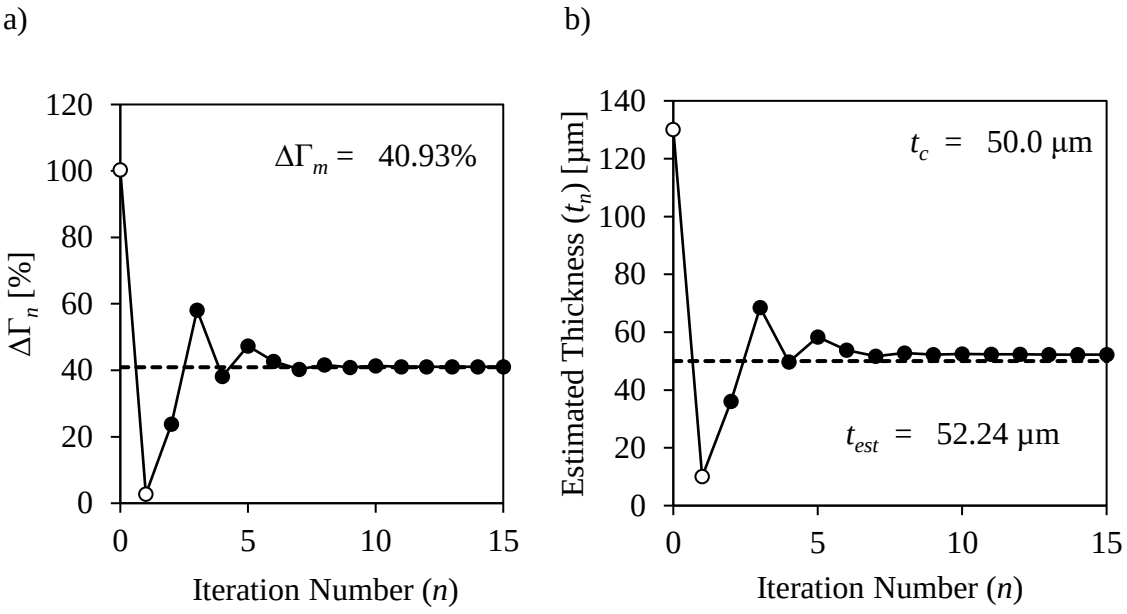

Figure 27. Simulated AECC change ($\Delta\Gamma_n$) iterations converging to the "measured" one and its corresponding coating thickness estimate using the single-frequency model.

4.5. Experimental System Setup

The system used for the experimental measurements is UniWest EddyView Premium eddy current measurement system that has an operating frequency range of up to 15 MHz. This range is generally suitable for all eddy current measurements [16]. Two eddy current probes with a spiral coil were used to acquire the AECC values for the frequency range of 0.1-15 MHz incremented logarithmically with a base of 10. The coil diameter for both coils was 3 mm. The first coil, which had an operating frequency of 100 kHz, covered a frequency range of 0.1-0.5 MHz and the second coil, which had an operating frequency of 2 MHz, covered the rest of the frequencies. The voltage data

from the EddyView system was acquired on the commercially available software LabView by National Instruments, where the AECC values were evaluated. Figure 29 shows the experimental setup used for AECC measurements.

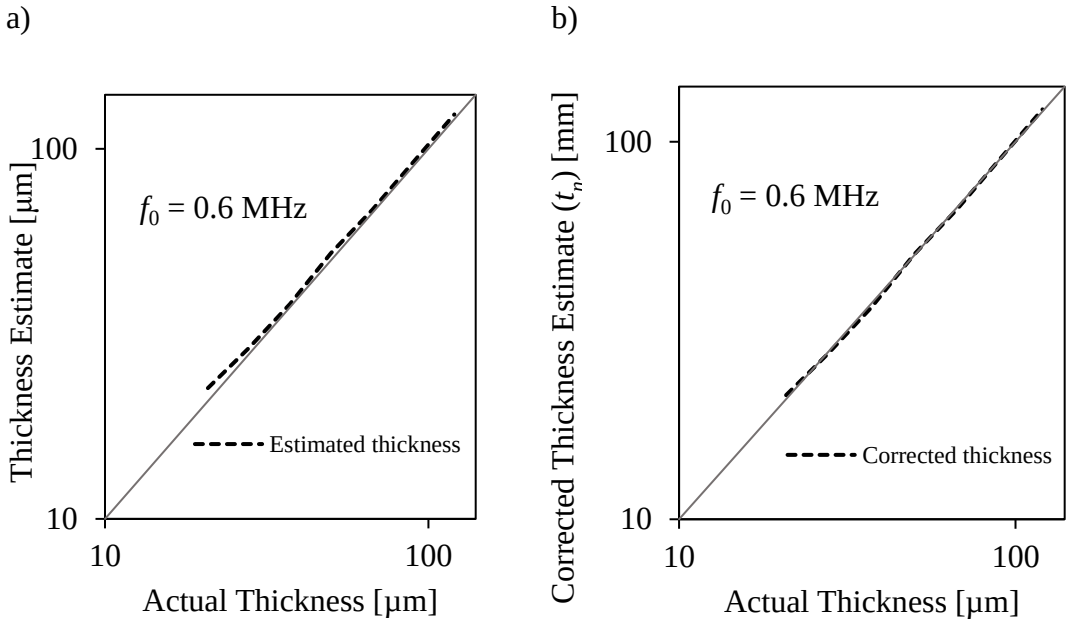

Figure 28. Coating thickness estimates for the entire coating thickness range of interest. Before and after applying a correction factor for the single-frequency inversion model.

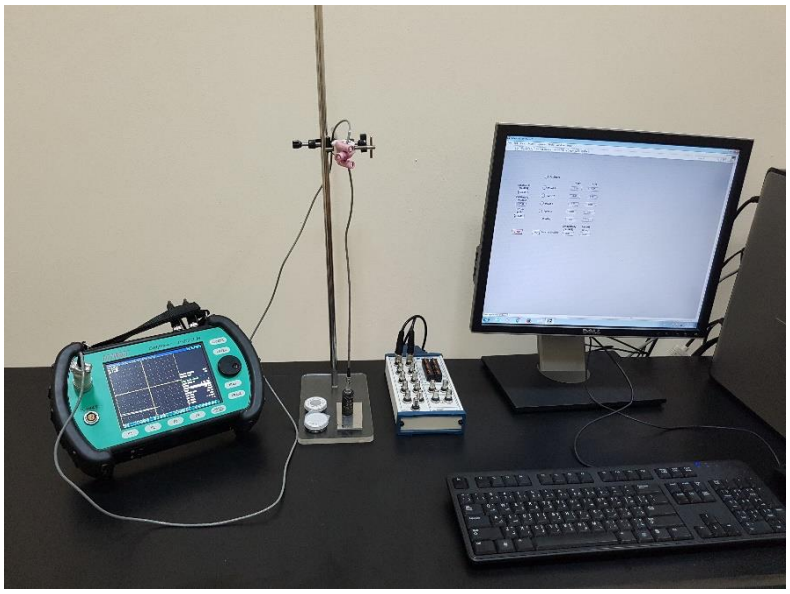

Figure 29. Experimental setup

4.6. Samples Used for Experimentation

Three samples of Al 1230 cladding over Al 2024 with unknown coating thicknesses were purchased from McMaster Carr. Each piece had an overall thickness of 3.2 mm. Each of the samples was cut such that the length and the width were both 38 mm. The substrate conductivity was measured from the side without cladding and had a value of 29.5 %IACS. After acquiring the AECC vales at all the frequencies the samples were cut at the point where the measurement was taken using Electrical Discharge Machining (EDM). To help in seeing the coating more clearly, the samples were first chemically etched using Kellers Etch which comprises of 190 ml water, 5 ml Nitric acid, 3 ml Hydrochloric acid and 2 ml Hydro fluoric acid. The samples were then placed under a Zeiss Smartproof light microscope under 5x magnification. Figure 30 shows the three samples as viewed from the microscope at 5x magnification. In each figure, it can be observed that there is a dark grey area that is in between the cladding and the substrate. This area is known as the heat affected zone [42].

The resulting AECC change for all three thicknesses is shown in Figure 31, where the solid line is the AECC spectrum obtained from the plane-wave approximation and the empty markers are the ones obtained from the experimental measurements. For the experiment 4 runs were conducted to acquire the AECC value for each frequency with each run having 23 values. The average of the four runs was determined to be the AECC value for a particular frequency. The value for the coating conductivity was obtained at 15 MHz where the eddy current standard penetration depth is small enough to only see the coating conductivity. These values were 58.74, 57.6 and 59.8 %IACS for the 67.9, 80.1 and 82.9 µm samples respectively. With all the parameters determined for each sample, the plane-wave approximation was used to generate the AECC spectrum for all three samples and were plotted along with the AECC values obtained from the experimental runs. From the figure it can be seen that the values obtained from the experiment and the plane-wave approximation are in agreement with each other.

4.7. Experimental Results

After obtaining the direct and indirect forward models, a comparative analysis was done for the two AECC-based inversion algorithms. Starting with spectroscopy AECC inversion model, Figure 32 shows the convergence of the simulated ($\Delta\Gamma_n$) AECC

spectrum to the "measured" one ($\Delta\Gamma_m$) and their corresponding coating thicknesses for each of the samples.

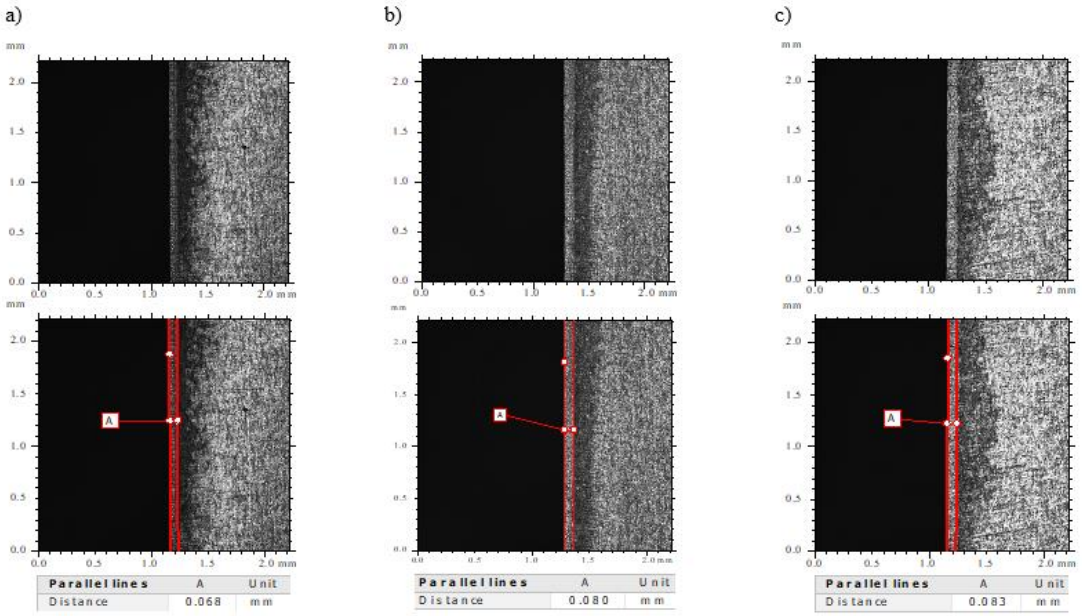

Figure 30. Al 1230 coating over Al 2024 substrate with coating thicknesses of 67.9 µm, 80.1 µm and 82.8 µm as viewed under a light microscope with 5x magnification

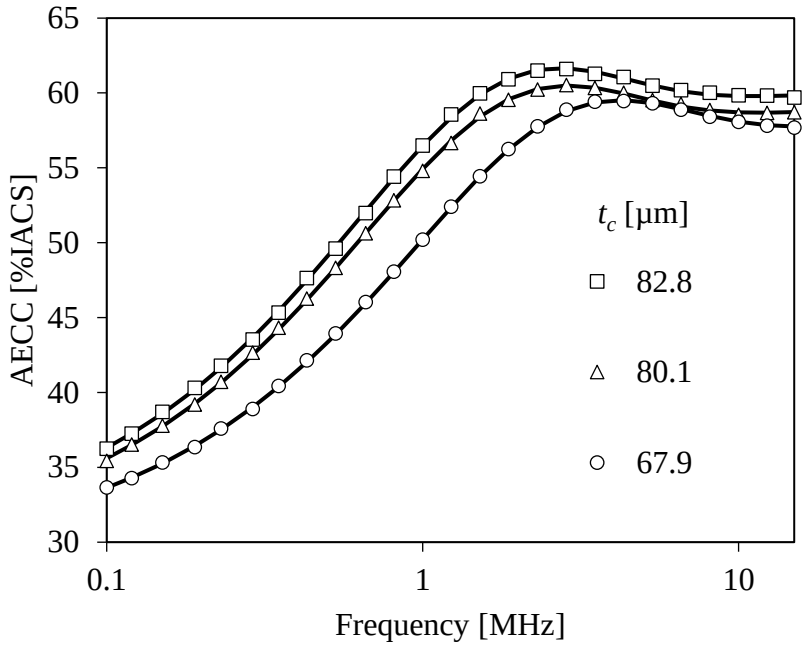

Figure 31. AECC values obtained through experiments (empty markers) with a coil diameter of 3-mm and the plane-wave approximation (solid lines) for three different coating thicknesses of Al 1230 coating over Al 2024 substrate.

Here it can be observed that the algorithm is reasonably accurate in estimating the coating thickness with the percentage error being less than 3% for COMSOL measurements and 1% for the experimental ones.

Moving on to the single frequency AECC inversion model, the measured AECC change was taken at the optimized frequency f_0 = 0.6 MHz. Starting with the lowest coating thickness and then moving up, the "measured" AECC changes for the three coating thickness were 53.57 68.15 and 71.74% as shown in Figure 33. Looking at the estimated coating thicknesses obtained from the single-frequency AECC inversion model, it can be seen that the coating thickness estimates are less accurate when compared to the spectroscopy AECC inversion model. However, the single-frequency model is still preferred as it is a much more practical model and the coating thickness estimates can be improved by using a correction factor using the same analysis done in the previous chapter.

Table 2 provides a summary of the coating thickness estimates with and without the correction factor for both the spectroscopy and single-frequency AECC inversion models. The table shows that after applying a correction factor, both inversion models offer negligible variance in estimating the coating thickness, making the single-frequency AECC inversion the preferred candidate for coating thickness estimation.

Table 2. Comparison between the Spectroscopy and Single-frequency AECC inversion models in accurately estimating coating thicknesses for the experimental runs.

Spectroscopy				**Single-frequency**			
t_{in} [µm]	t_{est} [µm]	t_{est}^{*} [µm]	error [%]	t_{in} [µm]	t_{est} [µm]	t_{est}^{*} [µm]	error [%]
67.9	67.35	68.52	0.913	67.9	67.08	67.94	0.059
80.1	80.57	80.01	0.112	80.1	79.72	80.04	0.075
82.8	82.51	82.94	0.169	82.8	82.03	82.67	0.157

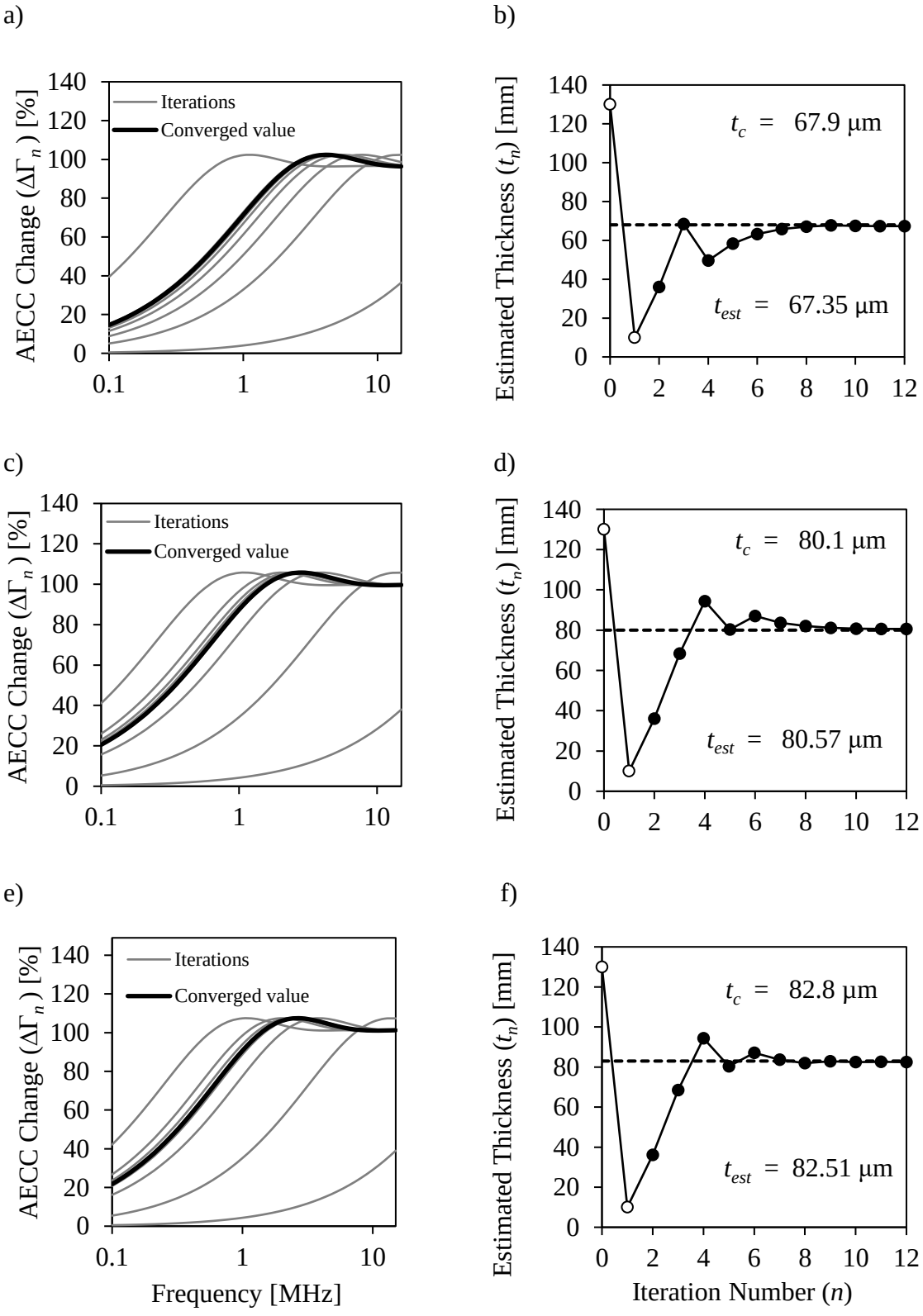

Figure 32. AECC change iterations (grey lines) with the converged spectrum (black line and their corresponding coating thickness estimates using the spectroscopy AECC inversion model

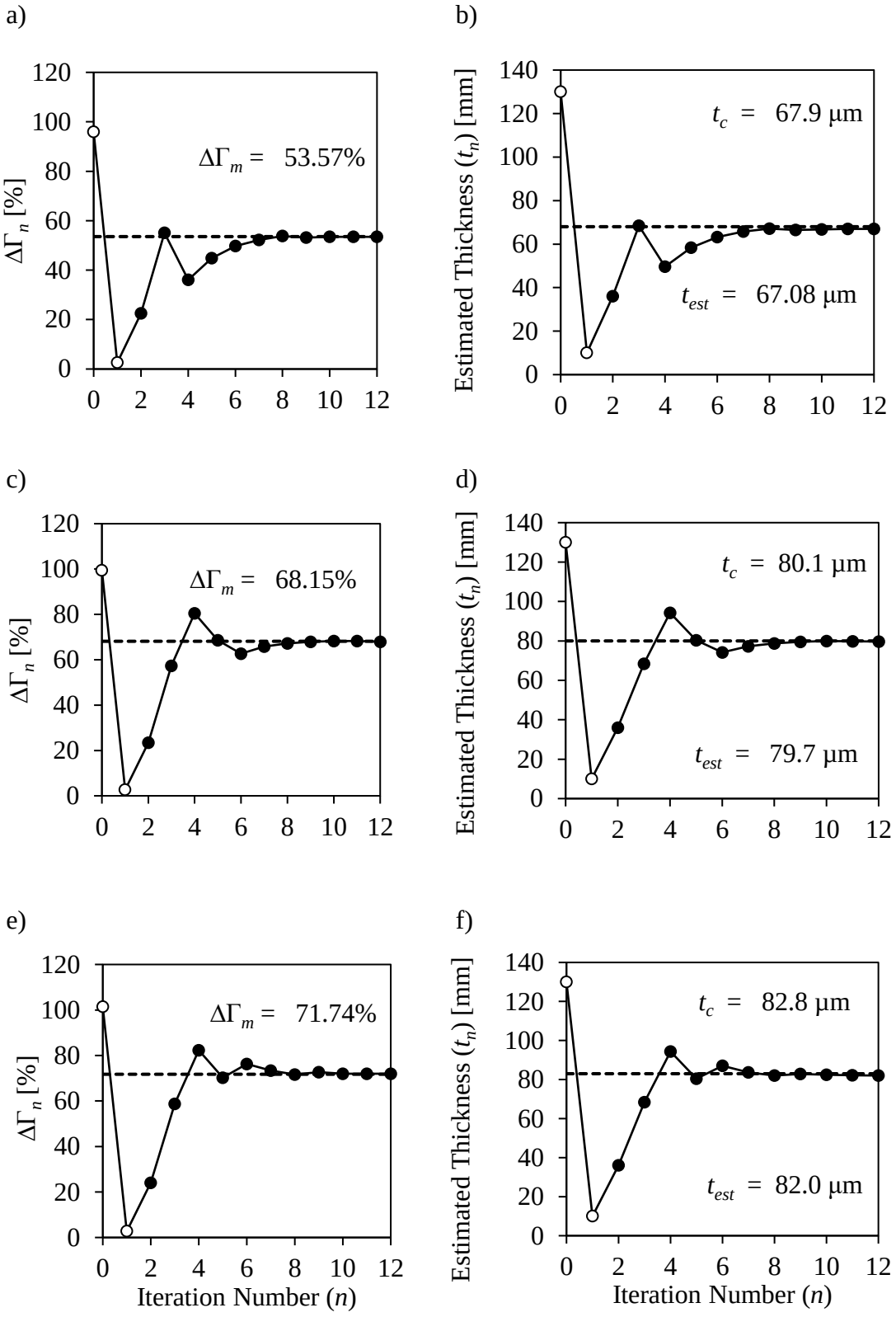

Figure 33. AECC change and their corresponding coating thickness estimates using the single-frequency AECC inversion model.

Chapter 5. Conclusion

The introduction of the recently developed AECC inversion model that used AECC spectroscopy to estimate metallic coating thickness over nonmagnetic metals showed the potential of using this technique for coating thickness estimation. However, certain technological constraints limited its ability to establish itself as a practical nondestructive evaluation technique for this purpose. Building on this study, a follow-up study was conducted to simplify the previously introduced spectroscopy AECC-based inversion model. This was achieved by taking AECC measurements at a single frequency obtained through an optimization analysis for a given coating/substrate combination. This optimized frequency allowed for a reduction in coil diameter as well as the number of calibration blocks required to calibrate the system. The follow up study paved the way for the development of an experimental technique for coating thickness estimation. This study develops an experimental technique to practically apply the recently introduced AECC-based inversion models to estimate the coating thickness of Al 1230 coating over Al 2024 substrate. These inversion models were tested experimentally and the accuracy obtained from each inversion models was compared for both cases. Although it was concluded that the spectroscopy AECC-based inversion model is slightly more accurate in estimating coating thickness, the implementation of correction factors yields the measurement uncertainty for both the models to be less than 1% for both inversion models. This low measurement uncertainty establishes the use of the single frequency AECC-based inversion model as an extremely powerful technique in estimating metallic coating thicknesses over nonmagnetic metals.

References

[1] J. Kawakita, H. Katanoda, M. Watanabe, K. Yokoyama, and S. Kuroda, "Warm Spraying: An improved spray process to deposit novel coatings," *Surface and Coatings Technology.*, vol. 202, no. 18 pp. 4369–4373, 2008.

[2] R. M. Molak, H. Araki, M. Watanabe, H. Katanoda, N. Ohno, and S. Kuroda, "Warm spray forming of Ti-6Al-4V," *Journal of Thermal Spray Technology*, vol. 23, no. 1–2, pp. 197–212, 2014.

[3] C. Sudha, P. Shankar, R. V. Subba Rao, R. Thirumurugesan, M. Vijayalakshmi, and B. Raj, "Microchemical and microstructural studies in a PTA weld overlay of Ni–Cr–Si–B alloy on AISI 304L stainless steel," *Surface and Coatings Technology.*, vol. 202, no. 10, pp. 2103–2112, 2008.

[4] ISO 21968:2005 Non-magnetic metallic coatings on metallic and non-metallic basis materials -- Measurement of coating thickness -- Phase-sensitive eddy-current method. Available: https://www.iso.org/standard/34781.html

[5] C. V. Dodd and W. E. Deeds, "Analytical solutions to eddy-current probe-coil problems," *Journal of Applied. Physics*, vol. 39, no. 6, pp. 2829–2838, 1968.

[6] J. W. Luquire, W. E. Deeds, and C. V. Dodd, "Alternating current distribution between planar conductors," *Journal of Applied. Physics*, vol. 41, no. 10, pp. 3983–3991, 1970.

[7] J. C. Moulder, E. Uzal, and J. H. Rose, "Thickness and conductivity of metallic layer from eddy current measurements," *Review of Scientific Instruments*, vol. 63, no. 6, pp. 3455–3465, 1992.

[8] Y. Takahashi, R. Urayama, T. Uchimoto, T. Takagi, H. Naganuma, K. Sugawara, and Y. Sasaki, "Thickness evaluation of thermal spraying on boiler tubes by eddy current testing," *International Journal of Applied Electromagnetics and Mechanics*, vol. 39, no. 1–4, pp. 419–425, 2012.

[9] F. Yu and P. B. Nagy, "Simple analytical approximations for eddy current profiling of the near-surface residual stress in shot-peened metals," *Journal of Applied Physics*, vol. 96, no. 2, pp. 1257–1266, 2004.

[10] B. A. Abu-Nabah, "Metallic coating thickness assessment over nonmagnetic metals using apparent eddy current conductivity spectroscopy," *International Journal of Applied Electromagnetics and Mechanics.*, vol. 54, no. 1, pp. 77–91, 2017.

[11] Y. Cheng, Y. Chen, J. Jiang, L. Bai, and B. Zhang, "Absorbing coating thickness measurement based on lift-off effect of eddy current testing," *International Journal of Applied Electromagnetics and Mechanics*, vol. 45, no. 1–4, pp. 323–330, 2014.

[12] C. Tai, J. H. Rose, and J. C. Moulder, "Thickness and conductivity of metallic layers from pulsed eddy-current measurements," *Review of Scientific Instruments.*, vol. 67, no. 11, pp. 3965–3972, 1996.

[13] Y. Cheng, L. Tian, C. Yin, X. Huang, and L. Bai, "A magnetic domain spots filtering method with self-adapting threshold value selecting for crack detection based on the MOI," *Nonlinear Dynamics*, vol. 86, no. 2, pp. 1–10, 2016.

[14] B. A. Abu-Nabah and P. B. Nagy, "Recent improvements in high-frequency eddy current conductivity spectroscopy," in *Review of Progress in Quantitative Nondestructive Evaluation*, 2008, vol. 27, pp. 392–399.

[15] B. A. Abu-Nabah and P. B. Nagy, "High-frequency eddy current conductivity spectroscopy for residual stress profiling in surface-treated nickel-base

superalloys," *NDT E Int.*, vol. 40, no. 5, pp. 405–418, 2007.
[16] B. A. Abu-Nabah and P. B. Nagy, "Lift-off effect in high-frequency eddy current conductivity spectroscopy," *NDT E International*, vol. 40, no. 8, pp. 555–565, 2007.
[17] B. A. Abu-Nabah, "Reduction of lift-off effect in high-frequency apparent eddy current conductivity spectroscopy," *Measurement Science and Technology*, vol. 28, no. 5, pp. 055107, 2017.
[18] B. A. Abu-Nabah and P. B. Nagy, "Iterative inversion method for eddy current profiling of near-surface residual stress in surface-treated metals," *NDT & E International*, vol. 39, no. 8, pp. 641–651, 2006.
[19] B. A. Abu-Nabah, W. T. Hassan, D. Ryan, M. P. Blodgett and P. B. Nagy "Eddy current residual stress profiling in surface-treated engine alloys" *NDT & E International* vol. 24 no. 1–2 pp. 209–232, 2009.
[20] B. A. Abu-Nabah and P. B. Nagy, "The feasibility of eddy current conductivity spectroscopy for near-surface cold work profiling in titanium alloys" *Review of Progress in Quantitative Nondestructive Evaluation* vol. 975 no. 1 pp. 1228–1235, 2008.
[21] B. A. Abu-Nabah, W. T. Hassan, D. Ryan, M. P. Blodgett and P. B. Nagy "The effect of hardness on eddy current residual stress profiling in shotpeened nickel alloys" *Journal of Nondestructuctive Evaluation* vol. 24 pp. 143–153, 2010.
[22] B. Abu-Nabah "Eddy current evaluation of metallic coating thicknesses over nonmagnetic metals" IOP Conf. Ser.: *Materials Science and Engineering*, 2018.
[23] M. P. Blodgett, B. A. Abu-Nabah, W. T. Hassan, P. B. Nagy "On the limitations of eddy current residual stress profiling in precipitation-hardened nickel-base superalloys" *Electromagnetic Nondestructive Evaluation* vol. 40, no. 5 pp. 405–418, 2007
[24] B. A. Abu-Nabah, W. T. Hassan, M. P. Blodgett, P. B. Nagy "Limitations of eddy current residual stress profiling in surface-treated engine alloys of various hardness levels" AIP Conference Proceedings, 2010
[25] B. A. Abu-Nabah and P. B. Nagy "Iterative inversion method of near-surface residual stress in surface-treated metals," AIP Conference Proceedings, 2007
[26] B. A. Abu-Nabah and P. B. Nagy "High-frequency eddy current spectroscopy for near surface residual stress profiling in surface-treated nickel-base superalloys," AIP Conference Proceedings, 2007
[27] G. Antonelli, M. Ruzzier, and F. Necci, "Thickness measurement of MCrAlY high-temperature coatings by frequency scanning eddy current technique," *Journal of Engineering for Gas Turbines and Power*, vol. 120, no. 3, pp. 537–542, 1998.
[28] V. Zilberstein, I. Shay, R. Lyons, N. Goldfine, T. Malow, and R. Reiche, "Validation of multi-Frequency eddy current MWM sensors and MWM-arrays for coating production quality and refurbishment assessment," in *ASME Proceedings: Manufacturing Materials and Metallurgy*, 2003, pp. 581–590.
[29] M. P. Blodgett and P. B. Nagy, "Eddy current assessment of near-surface residual stress in shot-peened nickel-base superalloys," *Journal of Nondestructuctive Evaluation*, vol. 23, no. 3, pp. 107–123, 2004.
[30] J. R. Bowler and S. J. Norton, "Eddy current inversion for layered conductors," *Research in Nondestructive Evaluation*, vol. 4, no. 4, pp. 205–219, 1992.
[31] E. Uzal and J. H. Rose, "The impedance of eddy current probes above layered metals whose conductivity and permeability vary continuously," *IEEE*

Transactions on Magnetics , vol. 29, no. 2, pp. 1869–1873, 1993.

[32] E. Uzal, J. C. Moulder, S. Mitra, and J. H. Rose, "Impedance of coils over layered metals with continuously variable conductivity and permeability: Theory and experiment," *Journal of Applied Physics*, vol. 74, no. 3, pp. 2076–2089, 1993.

[33] E. Uzal, J. C. Moulder, and J. H. Rose, "Experimental determination of the near-surface conductivity profiles of metals from electromagnetic induction (eddy current) measurements," *Inverse Problems*, vol. 10, no. 3, pp. 753–764, 1994.

[34] T. P. Theodoulidis, T. D. Tsiboukis, and E. E. Kriezis, "Analytical solutions in eddy current testing of layered metals with continuous conductivity profiles," *IEEE Transactions on Magnetics*, vol. 31, no. 3, pp. 2254–2260, 1995.

[35] I. T. Rekanos, T. P. Theodoulidis, S. M. Panas, and T. D. Tsiboukis, "Impedance inversion in eddy current testing of layered planar structures via neural networks," *NDT & E International*, vol. 30, no. 2, pp. 69–74, 1997.

[36] C. Glorieux, J. Moulder, J. Basart, and J. Thoen, "Determination of electrical conductivity profiles using neural network inversion of multi-frequency eddy-current data," *Journal of Physics D: Applied Physics*, vol. 32, no. 5, pp. 616–622, 1999.

[37] V. Sundararaghavan, K. Balasubramaniam, N. R. Babu, and N. Rajesh, "A multi-frequency eddy current inversion method for characterizing conductivity gradients on water jet peened components," *NDT & E International*, vol. 38, no. 7, pp. 541–547, 2005.

[38] W. Yin, S. J. Dickinson, and A. J. Peyton, "A multi-frequency impedance analysing instrument for eddy current testing," *Measurement Science and Technology*, vol. 17, no. 2, pp. 393–402, 2006.

[39] K. Kalyanasundaram and P. B. Nagy, "A simple numerical model of the apparent loss of eddy current conductivity due to surface roughness," *NDT & E International*, vol. 37, no. 1 pp. 47–56, 2004.

[40] Zain A. Ansari, Bassam A. Abu-Nabah, Maen Alkhader, "Single-frequency apparent eddy current conductivity assessment of metallic coating thicknesses over nonmagnetic metals", *International Journal of Applied Electromagnetics and Mechanics*, vol. 56, no. 4, pp. 533-547, 2018

[41] J. Davis, *Corrosion of aluminum and aluminum alloys*. Materials Park: ASM International, 2000, p. 203.

[42] G. Xie, Z. Luo, G. Wang, L. Li and G. Wang, "Interface Characteristic and Properties of Stainless Steel/HSLA Steel Clad Plate by Vacuum Rolling Cladding", *Materials Transactions*, vol. 58, no. 8, pp.1709–1712, 2011.

Vita

Zain Ali was born in 1996, in Mumbai, India. He received his primary and secondary education in Sharjah, UAE. He received his B.Sc. degree in Mechanical Engineering from the American University of Sharjah in 2016.

In September 2016, he joined the Mechanical Engineering master's program in the American University of Sharjah as a graduate teaching assistant. His research interests are in Non-destructive testing and Aviation.